

Demonstration of Algorithmic Quantum Speedup for an Abelian Hidden Subgroup Problem

Phattharaporn Singkanipa,¹ Victor Kasatkin,² Zeyuan Zhou,³ Gregory Quiroz,^{3,4} and Daniel A. Lidar⁵

¹*Department of Physics, University of Southern California, Los Angeles, CA 90089, USA*

²*Viterbi School of Engineering, University of Southern California, Los Angeles, CA 90089, USA*

³*William H. Miller III Department of Physics & Astronomy,*

Johns Hopkins University, Baltimore, Maryland 21218, USA

⁴*Johns Hopkins University Applied Physics Laboratory, Laurel, Maryland 20723, USA*

⁵*Departments of Electrical Engineering, Chemistry, Physics and Astronomy,*

and Center for Quantum Information Science & Technology,

University of Southern California, Los Angeles, CA 90089, USA

(Dated: January 17, 2024)

Simon’s problem is to find a hidden period (a bitstring) encoded into an unknown 2-to-1 function. It is one of the earliest problems for which an exponential quantum speedup was proven for ideal, noiseless quantum computers, albeit in the oracle model. Here, using two different 127-qubit IBM Quantum superconducting processors, we demonstrate an algorithmic quantum speedup for a variant of Simon’s problem where the hidden period has a restricted Hamming weight. The speedup is sub-exponential and is enhanced when the computation is protected by dynamical decoupling to suppress decoherence. The speedup is further enhanced with measurement error mitigation. This constitutes a demonstration of a bona fide quantum advantage for an Abelian hidden subgroup problem.

I. INTRODUCTION

Quantum algorithms have been known to outperform classical algorithms for more than 30 years [1–13], assuming that they run on ideal, noiseless quantum devices. However, today’s noisy intermediate-scale quantum (NISQ) [14] devices are functional on a relatively small scale of several hundreds of qubits and are highly susceptible to performance degradation due to decoherence and control errors. A central current focus is the experimental demonstration of an algorithmic quantum speedup on these devices, i.e., a scaling advantage for a quantum algorithm solving a computational problem. A variety of such demonstrations have been reported [15–25], but all are subject to various caveats such as relying on computational complexity conjectures or being limited to an advantage over a restricted set of classical algorithms. These demonstrations are separate and distinct from recent quantum supremacy results [26–31] and from benchmarking the performance of NISQ devices [32–36]. The former does not corroborate a scaling advantage [37–39], while the latter focuses on demonstrating better-than-classical probabilities of success without resolving the question of scaling of the time to solve the computational problem with problem size, which is essential for the demonstration of an algorithmic quantum speedup [40].

Recently, a conjecture-free algorithmic quantum speedup was demonstrated in the oracle model against the best possible classical algorithm [41]. In particular, a polynomial algorithmic quantum scaling advantage for the single-shot version of the Bernstein-Vazirani algorithm was observed when implemented on a 27-qubit IBM Quantum processor with noise suppression via dynamical decoupling (DD) [42–44], a well-established error suppression method for NISQ devices [45–49]. The Bernstein-Vazirani algorithm was among the very first algorithms for which a quantum speedup was rigorously proven, and in this sense, it is of historical significance. Even more interesting would be an algorithmic quantum speedup

for a problem that belongs to the class of Abelian hidden subgroup problems [50], which includes integer factorization. Simon’s problem [3], a precursor to Shor’s factoring algorithm [5], involves finding a hidden subgroup of the group (\mathbb{Z}_2^n, \oplus) , which is the n -fold direct product of the cyclic group \mathbb{Z}_2 (the integers modulo 2) with the group operation being bitwise XOR (\oplus), and this group is Abelian. In Simon’s problem, the Abelian hidden subgroup consists of the identity and a secret string b , and the goal is to determine b .

Here, we revisit Simon’s problem and demonstrate an unequivocal algorithmic quantum speedup for a restricted Hamming-weight version of this problem using a pair of IBM Quantum processors. Similar to Ref. [41], we find an enhanced quantum speedup when the computation is protected by DD. The use of measurement error mitigation (MEM) further enhances the scaling advantage we observe. Our result can be viewed as bringing the field of NISQ algorithms closer to a demonstration of a quantum speedup via Shor’s algorithm. It also highlights the essential role of quantum error suppression methods in such a demonstration.

To set the stage, we now explain the restricted-weight Simon’s problem that is the focus of this work. In the original formulation of Simon’s problem, we are given a function $f_b : \{0, 1\}^n \rightarrow \{0, 1\}^n$, where n is the problem size, and we are promised that f_b is either 1-to-1 or 2-to-1, such that $\forall x, y \in \{0, 1\}^n, f_b(x) = f_b(y)$ if and only if $x = y$ or $x = y \oplus b$ for a hidden bitstring $b \in \{0, 1\}^n$. We wish to determine which condition holds for f_b and, in the latter case, find b . Since the first condition (1-to-1) has one possible hidden bitstring $b = 0^n$, in this work we only consider the 2-to-1 version of Simon’s problem, and our goal is to determine the length- n hidden bitstring b . It is well known (and we revisit this below in detail) that the classical and quantum query complexities are $O(2^{n/2})$ and $O(n)$, respectively.

Instead of allowing all possible binary hidden bitstrings $b \in \{0, 1\}^n$ as in the original Simon’s problem, we restrict their Hamming weight (HW), that is, the number of 1’s in b .

We refer to this modification as the ‘restricted-HW’ version of Simon’s algorithm, denoted w_w Simon- n . Here $w \leq n$ is the maximum allowed HW. We will show that this modification allows us to exhibit a quantum speedup for relatively shallow circuits, whose depth is set by w . The need for the restriction arises because current NISQ devices are still too noisy to fully solve the original, unrestricted ($w = n$) Simon’s problem when n becomes large.

We work in the setting of a guessing game, the rules of which are tuned in order to make the speedup possible and are explained in Section II. In particular, we introduce an oracle-query metric we call NTS (number-of-oracle-queries-to-solution), to quantify the performance of different players of this game. The optimal classical and quantum algorithms to solve Simon’s problem are described in Section III. We show that the classical algorithm requires $\text{poly}(n^{w/2})$ oracle queries, whereas the quantum algorithm requires $\sim w \log_2(n)$ queries. In Section IV we quantify how a quantum speedup can be detected using the NTS metric. In Section V we discuss the experimental setup and IBMQ devices we used to perform our algorithmic speedup tests, including the DD sequences we selected to enhance performance. Then, in Section VI we discuss our results and the evidence for a quantum speedup in the w_w Simon- n problem. We conclude in Section VII. The appendices contain additional technical details as well as supplemental experimental results.

II. RULES OF THE GAME

The game is designed for a single player. If there are multiple players, they can play the game individually and then compare their scores. At a high level, the game works as follows. A function $f: \{0,1\}^n \rightarrow \{0,1\}^n$ that satisfies the 2-to-1 condition is chosen uniformly at random. The function is not known to the player, but the player has oracle access to compute $f(x)$ for any $x \in \{0,1\}^n$. For classical players, oracle access means that the player can send a query x to the oracle and receive $f(x)$ in return. For quantum players, we define a unitary \mathcal{O}_f such that $\mathcal{O}_f |x\rangle |a\rangle = |x\rangle |a\rangle |a \oplus f(x)\rangle$. The player performs a certain number of such oracle queries and arbitrary classical computations and then guesses the hidden bitstring b . The correctness of the guess is checked, and a new round begins, i.e., a new function is chosen, and the game is repeated. The goal of the player is to maximize the number of correct guesses using the smallest number of oracle queries.

The rest of this section is devoted to specifying the details missing in the simplified description above: the set of functions f , the mechanism to access the oracle, and the exact formula used to score the player.

A. Set of functions f

We would like to design a game that is hard for a classical computer and easy for a quantum computer. The classical complexity lower bound (see Section IIIA) is based on the

assumption that the only information about b that the classical player can extract by evaluating f at various points is the presence or absence of a match $f(x) = f(y)$ for pairs of queries (x, y) . In w_w Simon- n , the conditions are as follows: (i) $\text{HW}(b) \leq w$; (ii) $f(x) = f(y)$ if and only if $x = y$ or $x = y \oplus b$; and (iii) $b \neq 0^n$. The function f is then chosen uniformly at random from the set of all functions that satisfy these conditions. Such a broad class of functions f may seem overly complicated, but to illustrate the importance of this choice, consider an extreme alternative: b is chosen uniformly from all bitstrings that satisfy conditions (i) and (iii), and $f(x) = \min(x, x \oplus b)$, where \min yields the first bitstring in lexicographic ordering. In this case, since $f(1^n) = 1^n \oplus b$, we have $b = 1^n \oplus f(1^n)$. Therefore, the classical player can find b in a single query: $x = 1^n$.

Unfortunately, choosing f uniformly at random from the set of all functions that meet conditions (i)–(iii) leads to a problem. To select a function we need to pick its value for each pair of inputs x and $x \oplus b$. There are 2^{n-1} such pairs and 2^n possible outputs, all of which should be different. One way to compute the number of such functions is to first pick one of the $\binom{2^n}{2^{n-1}}$ subsets as the image of f and then one of the $(2^{n-1})!$ ways to map 2^{n-1} inputs to 2^{n-1} outputs, giving the total number of functions f for a fixed b as $\binom{2^n}{2^{n-1}}(2^{n-1})! = 2^n!/(2^{n-1})! > 2^{(n-1)2^{n-1}}$, which means that the choice of f requires at least $(n-1)2^{n-1}$ encoding bits. One would thus expect exponentially many gates to be required to implement the unitary quantum oracle \mathcal{O}_f in a quantum circuit. Such large circuits are infeasible on NISQ devices. To circumvent this problem, we introduce the notion of a compiler that preserves the shallowness of the quantum circuits implementing \mathcal{O}_f but prevents making the problem trivial by offloading all computations to classical post-processing. The details of this compiler are given in Appendix A. The corresponding Simon’s oracle construction is described in Appendix B.

B. Scoring

Any function f satisfying (i)–(iii) can be decomposed as $f(x) = f_1(f_0(x))$, where f_0 is any 2-to-1 function satisfying condition (ii) with the same b , and f_1 is a permutation of bitstrings. A uniformly random f can be obtained by fixing $f_0 = f_{0b}$ for every b , then picking b and f_1 uniformly at random. Since exponentially many bits are required to record the permutation f_1 , the program to compute f_1 occupies exponential memory. If no caching is involved, this program would need to be loaded into memory every time, which takes exponential time in n . Thus, classical post-processing may easily remove most of the quantum advantage. To circumvent this, we introduce a scoring function that only accounts for the number of oracle queries and ignores the time needed for all other steps of the protocol.

Given the goal of maximizing the number of correct guesses of b while minimizing the number of oracle queries, the players’ performance can be measured in terms of the av-

verage score per query, which we denote by NTS^{-1} , where

$$\text{NTS} = \frac{\langle Q \rangle}{\langle P \rangle}. \quad (1)$$

Here NTS denotes the *number-of-oracle-queries-to-solution*, $\langle \bullet \rangle$ denotes the expectation value (which can be obtained as an average over many rounds of the game), Q is the number of oracle queries, and P is the score obtained in a round. The best player is the one with the highest NTS^{-1} .

Naively, one could set $P = 1$ if the guess is correct and $P = 0$ otherwise. However, this would allow the players to use the following strategy. Let N be the total number of options for b , and let C be a constant satisfying $N \geq C > 0$. With probability C/N , the player executes a single query and discards the result; otherwise, 0 queries are executed. Then the player guesses b uniformly at random. The expected score is $1/N$, and the expected number of queries is C/N . Thus, $\text{NTS} = C$, and the player can make NTS arbitrarily small (e.g., $\text{NTS} = 1$) by picking C small enough.

To avoid this, we introduce a penalty for incorrect guesses. Let $p_r = 1/N$ be the probability of a random b being correct. Then we set $P = 1$ if the guess is correct and $P = -p_r/(1-p_r)$ otherwise. This ensures that the randomly guessing player has $\langle P \rangle = p_r \times 1 + (1-p_r) \times [-p_r/(1-p_r)] = 0$ and $\text{NTS} = \infty$.

To recap, we focus on counting the number of oracle calls for two main reasons: (i) optimizations performed by the compiler may change the time significantly, and (ii) the data generated by NISQ devices, contrary to classical and ideal quantum algorithms, requires non-trivial post-processing, which is likely to destroy any quantum speedup we might otherwise derive from such devices.

III. CLASSICAL AND QUANTUM ALGORITHMS

We now explain in detail the algorithms for the different variants of the algorithm we consider: (i) classical, (ii) noiseless quantum, (iiia) NISQ, and (iiib) NISQ without measurement errors, simulated using measurement error mitigation (MEM).

We first comment briefly on the quantum variants. In the *noiseless quantum* case, an ideal gate-based quantum computer executes the circuit the player designs. Whether any compilation is performed is irrelevant to determining the optimal score since such a compilation does not affect the number of oracle calls or the probability distribution of the outcomes of the circuit execution returned to the player. In the *NISQ* case, we run the compiled circuit on a NISQ device and, after post-processing, return the result to the player. The score a player receives in this case depends not only on the player's strategy but also on the NISQ device used. In the *NISQ without measurement errors* case, we run the circuit multiple times and use MEM to estimate the probability distribution we would have obtained from a single run if measurement errors were absent. Then we sample from that probability distribution, apply the post-processing, and return the result to the player.

From the standpoint of the player, the procedure for implementing the 'NISQ' and 'NISQ with MEM' variants remains identical. This is due to MEM being processed within the compiler, with the observer receiving solely the outcome, presumed to incorporate measurement errors (NISQ) or devoid of such errors (NISQ with MEM).

A. Classical algorithm

The original Simon's problem can be solved using a classical deterministic algorithm in $O(2^{n/2})$ queries [3, 51]. We present a derivation of this result here and generalize it to the setting of the w_w Simon- n problem. For a simplified but less rigorous derivation, see Appendix C.

Let S be the set of all possible values for the hidden bitstring $b \neq 0^n$. The size of this set is $N_n \equiv 2^n - 1$. Consider a classical player querying bitstrings x_1, x_2, \dots, x_k to get values y_1, \dots, y_k , where $y_j = f(x_j) \in \{0, 1\}$. Having made m queries, the player forms the set $R_m = \{x_j \oplus x_l : 1 \leq j < l \leq m\}$. If $b \in R_m$, then $b = x_j \oplus x_l$ for some $j, l \leq m$ and $y_j = y_l$. In this case, the player knows b and their best strategy is to output it without further queries to the oracle. Under the assumption that f is a uniformly random function satisfying conditions (i)–(iii) discussed in Section II, if $b \notin R_m$, then the only information learned after m queries is that b is not in R_m . Thus, the player cannot benefit from adjusting the sequence of queried bitstrings based on the learned information and can assume that the classical algorithm is fully described by the sequence x_1, x_2, \dots, x_k . Finally, one can check that the NTS cannot be improved by guessing prematurely. Hence, for an optimal algorithm, the player should know b after all k queries, i.e., $S \setminus R_k$ should contain at most one element. On the other hand, $|R_k| \leq k(k-1)/2$. I.e., k should satisfy

$$\frac{k(k-1)}{2} \geq N_n - 1. \quad (2)$$

We now consider w_w Simon- w , where the set S of possible values of b is restricted by $\text{HW}(b) = w < n$. The size of this set is

$$N_w \equiv \sum_{j=1}^w \binom{n}{j}. \quad (3)$$

Let $S_k = S \cap R_k$. Similar to the above, if $b \notin S_k$, then this is the only information about b available to the player, i.e., their posterior distribution of all possible values of b is uniform in $S \setminus S_k$. The player is guaranteed to know the correct b iff $S \setminus S_k$ contains at most one element, i.e., $|S_k| \geq N_w - 1$, but $|S_k| \leq |R_k| \leq k(k-1)/2$. Hence,

$$\frac{k(k-1)}{2} \geq N_w - 1. \quad (4)$$

Solving Eq. (4) for k , we obtain a lower bound on the worst-case number of queries needed by the classical player to solve w_w Simon- n :

$$k \geq \left\lceil \sqrt{2N_w - \frac{7}{4}} + \frac{1}{2} \right\rceil \equiv k_{\min}(N_w), \quad (5)$$

where, since this result is for a deterministic classical algorithm, it is also a lower bound on the worst-case classical NTS.

Equation (1), however, involves not the worst-case but the average number of queries $\langle Q \rangle$. The lower bound on the expected number of classical queries $\langle Q_C \rangle$ needed to know b exactly can be obtained by summing the lower bounds on the probability $b \notin S_i$. Since there are at most $i(i-1)/2$ elements in S_i , and the total number of possible b values is N_w , we have $\Pr(b \in S_i) \leq \frac{i(i-1)}{2N_w}$. The probability that the next query $\#i+1$ is needed (i.e., that i queries are not enough: $i = 0, \dots, k-1$) is $1 - \Pr(b \in S_i)$. Thus,

$$\langle Q_C \rangle \geq \sum_{i=0}^{k-1} \left(1 - \frac{i(i-1)}{2N_w}\right) = k - \frac{k(k-1)(k-2)}{6N_w}. \quad (6)$$

As mentioned above, guessing b when it is unknown to the classical player does not increase the NTS; hence, the lower bound on the classical NTS $\equiv \text{NTS}_C = \langle Q_C \rangle / \langle P_C \rangle \geq \langle Q_C \rangle$ is given by the r.h.s. of Eq. (6). Combining this with Eq. (5) gives

$$\text{NTS}_C \geq \text{NTS}_C^{\text{lb}}(N_w) \equiv k_{\min} - \frac{k_{\min}(k_{\min}-1)(k_{\min}-2)}{6N_w} \quad (7)$$

as the lower bound on the average case classical NTS.

Note that $\binom{n}{w} \leq N_w \leq \min(w\binom{n}{w}, 2^n - 1)$. Thus, for constant w (independent of n), $N_w \sim n^w$, $k_{\min} \sim n^{w/2}$, and Eq. (7) yields $\text{NTS}_C \sim n^{w/2}$. Without restricting $\text{HW}(b)$, $\text{NTS}_C = O(2^{n/2})$. However, with a fixed upper limit w on $\text{HW}(b)$, NTS_C is polynomial asymptotically (as $n \rightarrow \infty$).

Although Eq. (7) lower-bounds NTS_C , there is no guarantee that the player will find a sequence of bitstrings $x = \{x_1, x_2, \dots, x_k\}$ that achieves it. Nevertheless, henceforth we use the lower bound given by Eq. (7) as the metric for NTS_C because if the quantum algorithm defeats this lower bound, the implication is an unequivocal quantum speedup. In Appendix D, we derive an upper bound on NTS_C and discuss the gap between the lower and upper bounds.

B. Noiseless quantum algorithm

The original Simon- n problem can also, in theory, be solved on a noiseless quantum computer (QC). Figure 1 shows a quantum circuit that executes this algorithm. The circuit uses $2n$ qubits for w_w Simon- n ; the first n are data qubits, labeled d_j , and the other n are ancilla qubits, labeled a_j , where $j = 0, 1, \dots, n-1$. The box \mathcal{O}_b is the oracle whose action is $f_b(x)$ on an input x , but its circuit is hidden from the players. Each execution of the circuit produces a uniformly random z such that $z \cdot b = 0$. The well-known proof that $O(n)$ executions of this circuit (on average) on an ideal quantum computer are sufficient for solving Simon- n is given in Appendix E for completeness.

For our purposes, we need the NTS for the noiseless quantum w_w Simon- n problem, for arbitrary w . More precisely, we need the NTS for an optimal, ideal quantum player executing the circuit in Fig. 1 until $b \in S$ can be uniquely determined,

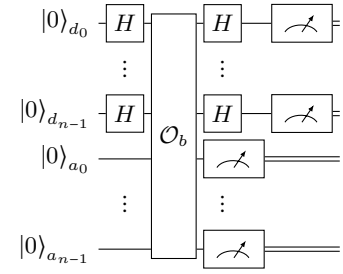


FIG. 1. Quantum circuit for solving Simon's problem with a length- n hidden bitstring b . The structure of the oracle \mathcal{O}_b is not visible to the player who wishes to guess b . The top n measurement results form the bitstring z , and the bottom n measurement results are discarded in the algorithm.

which we denote by NTS_{IQ} for ‘ideal quantum’. To obtain this, we first consider a generalization of the w_w Simon- n problem to the case where b is known to belong to some subset S of $\mathbb{Z}_2^n \setminus \{0^n\}$, and obtain NTS_{IQ} exactly in the two limits $w = 1, \infty$, after which we construct NTS_{IQ} for arbitrary $1 < w < \infty$ via interpolation.

Theorem 1. *If $|S| = 1$ then $\text{NTS}_{\text{IQ}} = 0$. If $|S| \geq 2$ then*

$$\log_2 |S| \leq \text{NTS}_{\text{IQ}} \leq \log_2(|S| - 1) + 2. \quad (8)$$

For w_w Simon- n , we have $|S| = N_w$. For Simon- n (i.e., w_∞ Simon- n), $|S| = 2^n - 1$ and

$$\text{NTS}_{\text{IQ}} = \sum_{k=1}^{n-1} \frac{1}{1 - 2^{-k}} = n + E_{\text{EB}} - 1 + O(2^{-n}), \quad (9)$$

where $E_{\text{EB}} = 1.60669 \dots$ is the Erdős-Borwein constant [52]. For w_1 Simon- n , $|S| = n$ and

$$\text{NTS}_{\text{IQ}} = \log_2(n) + \frac{1}{2} + \frac{\gamma}{\ln(2)} + \chi(\log_2(n)) + O\left(\frac{1}{n}\right), \quad (10)$$

where $\gamma = 0.57721 \dots$ is the Euler-Mascheroni constant and χ is a small ($\ll 1$) periodic function with mean 0.

The proof is given in Appendix F. Numerically, we estimate the amplitude of χ in Eq. (10) as 1.58×10^{-6} .

We now construct the aforementioned interpolation. Let $t \equiv N_w / (2^n - 1)$; t represents the density of b 's in the space of all non-zero bitstrings. In Eq. (9) $t = 1$ and in Eq. (10) t approaches 0. The interpolation between Eqs. (9) and (10) is then:

$$\text{NTS}_{\text{IQ}}(t) = \log_2(N_w) + \left(\frac{1}{2} + \frac{\gamma}{\ln(2)}\right)(1-t) + (E_{\text{EB}} - 1)t. \quad (11)$$

Appendix G demonstrates that this interpolation is an accurate estimate of the actual NTS_{IQ} for the w_w Simon- n problem when $1 < w < \infty$.

C. NISQ algorithm

The ‘NISQ algorithm’ executes the circuit depicted in Fig. 1 on a NISQ device. Recall that to determine the correct hidden

bitstring b in the context of a noiseless quantum algorithm, it is necessary to acquire a set of $n - 1$ independent measurements z , all of which satisfy the condition $z \cdot b = 0$. However, in the presence of noise, the measurement outcomes from the first n qubits are expected to deviate from the noiseless case, potentially leading to incorrect values for z . The likelihood of obtaining at least one incorrect z increases as the problem size n increases, and given the prevailing noise levels in current NISQ devices, the probability of encountering at least one erroneous z is high even for relatively small problem sizes. Consequently, attempting to determine the parameter b based solely on $n - 1$ measurements is highly likely to yield an incorrect solution.

As a remedy, we employ a modified algorithm that requires $O(n)$ measurements, thereby increasing the robustness of the determination of b . The algorithm aims to identify a unique binary string b' by sampling bitstrings z and scoring each b' based on the condition $z \cdot b' = 0$. While theoretically, $O(n)$ samples should suffice to determine b , the algorithm samples $O(kn)$ bitstrings to mitigate errors in z , with k being a constant independent of n . Each sampled z is tested against all candidate b' strings, incrementing the score of b' that satisfies the dot product condition. After processing kn samples, the algorithm selects the b' with the highest score. In case of a tie, additional z samples are used until a single b' stands out. This method is robust to noise, allowing for the correct b to be discerned even when some sampled z 's are corrupted, provided that the noise does not lead to a uniform score distribution. For a complete description, see Appendix H.

We subject the outcomes from the ‘NISQ’ and ‘NISQ with MEM’ algorithms to identical post-processing methodologies. The speedup comparison between the classical and quantum algorithms uses the better of the outcomes observed between these two quantum variants.

IV. QUANTUM SPEEDUP QUANTIFIED

In Section II B, we motivated and defined the NTS metric, which we use to compare the number of oracle queries for classical and NISQ solutions to Simon’s problem. Instead of computing the NTS for all possible oracles \mathcal{O}_f , or even for all N_w values of b , we note that our NISQ implementation for w_w Simon- n depends only on n, w , and the Hamming weight $HW(b) = i$, which allows us to focus only on $w \leq n$ instances of b : one representative b for each i . For full details, see the reduction method described in Appendix I.

Let $h_i = \binom{n}{i}$ be the corresponding number of length- n bitstrings b and let Q_i be the corresponding total number of oracle queries; we can write the number of queries for a given i as $h_i Q_i$, and thus the total number of queries per hidden bitstring as $\langle Q \rangle = \sum_{i=1}^n h_i Q_i / N_n$. Let p_i be the probability of the correct guess for a representative bitstring b with $HW(b) = i$. That is, p_i is the fraction of successful guesses of the representative b based on the Q_i oracle calls. Assuming all h_i bitstrings of fixed Hamming weight i are guessed with the same probability p_i , the total probability of successfully guessing all weight- i bitstrings is $h_i p_i$, and the expected overall proba-

bility of success over all bitstrings is $\langle p \rangle = \sum_{i=1}^n h_i p_i / N_n$. In the restricted w_w Simon- n version, since the player knows w , a random guess succeeds with probability $p_r = 1/N_w$, where N_w replaces N_n . Then the average score (which includes the penalty for incorrect guesses and was defined in Section II B) can be written as $\langle P \rangle = \langle p \rangle \times 1 + (1 - \langle p \rangle) \times [-p_r / (1 - p_r)] = \langle p \rangle - (1 - \langle p \rangle) / (N_w - 1) = \frac{1}{N_w - 1} (N_w \langle p \rangle - 1)$. We can now express the quantum NTS for the unrestricted ($w = n$) or restricted ($w < n$) version of Simon’s problem as:

$$\text{NTS}_Q(n; w) = \frac{\langle Q \rangle}{\langle P \rangle} = \frac{N_w - 1}{N_w} \frac{\sum_{i=1}^w h_i Q_i}{\sum_{i=1}^w h_i p_i - 1}. \quad (12)$$

Recall that we need to compare NTS_Q to the lower bound on the average-case classical NTS, i.e., NTS_C^{lb} given by Eq. (7), which is a simple function of $k_{\min}(N_w)$, the lower bound on the worst-case classical NTS given by Eq. (5). Since $k_{\min}(N_w) \sim N_w^{1/2}$ for $N_w \gg 1$, it is more convenient to define the NTS scaling with respect to N_w than n .

We can now define an *algorithmic quantum speedup* for the w_w Simon- n problem as a better scaling with N_w of the function NTS_Q [Eq. (12)] than the function NTS_C^{lb} [Eq. (7)]. We determine the scaling by fitting the following two-parameter model:

$$\log_2 \text{NTS}_x = a_x \log_2 N_w + c_x, \quad x \in \{Q, C\}, \quad (13)$$

where a_x is the scaling exponent. An *algorithmic quantum speedup* is observed when $a_Q < a_C$ for a fixed w . The fitting parameter c_x does not matter for scaling purposes.

Note that Eq. (13) relates two logarithmic quantities; hence, the quantum speedup it quantifies is subexponential.

V. EXPERIMENTAL IMPLEMENTATION

Our experiments were conducted using the 127-qubit devices Sherbrooke (ibm_sherbrooke) and Brisbane (ibm_brisbane), as well as the 27-qubit devices Cairo (ibm_cairo) and Kolkata (ibmq_kolkata), whose specifications are detailed in Appendix J.

The quantum circuit for each hidden bitstring b was constructed according to Fig. 1, then compiled to fit the architecture of the devices using the as-late-as-possible (ALAP) schedule. This schedule initializes each qubit just before its first operation. We performed our experiments in two main modes: (i) ‘with DD’, i.e., error-suppressed experiments with different dynamical decoupling sequences, and (ii) ‘without DD,’ i.e., the circuit as specified in Fig. 1 without any additional error suppression.

We use a pre-compiled quantum circuit aligned with the underlying device architecture as our base circuit. The base circuit contains idle gap periods, suitable for the integration of DD sequences. We incorporated one iteration of a DD sequence into each idle gap, with the condition that if the duration of the period is insufficient for sequence inclusion, the gap remains unoccupied [41]. The spacing of DD pulses is contingent upon both the length of the idle gap and the total

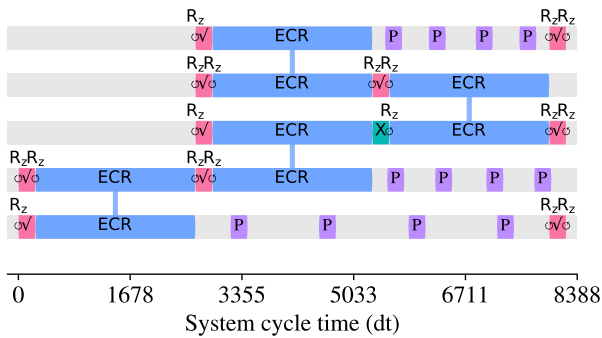


FIG. 2. Circuit for Simon-3 ($b = 111$) compiled into the Sherbrooke architecture using the ALAP schedule. The XY4 DD sequences shown here as an example are placed such that they fill all available idle spaces after each qubit is initialized. Pulse intervals vary depending on the length of the idle period. \sqrt{X} denotes the \sqrt{X} gate. ECR denotes an echoed cross-resonance gate, which is equivalent to a CNOT up to single-qubit rotations.

number of pulses of the DD sequence. The compiled Simon-3 circuit ($b = 111$) is depicted in Fig. 2. The idle intervals within this circuit are schematically populated with a 4-pulse DD sequence denoted by “P” in purple boxes.

We thoroughly examined a broad set of DD sequences: $\mathcal{D} = \{\text{CPMG}, \text{RGA}_{2x}, \text{XY4}, \text{UR}_6, \text{RGA}_{8a}, \text{UR}_{10}, \text{RGA}_{16b}, \text{UR}_{18}, \text{UR}_{26}, \text{RGA}_{32a}, \text{RGA}_{32c}, \text{UR}_{32}\}$. These sequences were selected from a comprehensive array of sequences investigated in Ref. [53] on 1-5 qubit IBMQ devices, which includes detailed descriptions of these sequences and concluded that sequence performance is highly device- and metric-dependent. Based on these findings, our sequence-selection process involved iterative experimentation, with smaller-scale trials conducted repeatedly to discern sequences that, on average, exhibited superior performance compared to others. We also investigated the crosstalk-robust sequences proposed in Ref. [54].

Certain sequences, such as UR_m [55] and RGA_m [56], are families depending on a parameter m , which (roughly) counts the number of pulses and the corresponding error suppression order; we optimized over m and chose the best-performing sequences for the final experiment. The optimization procedure we used relies on the NTS metric. Subsequently, circuits incorporating idle periods, each filled with a specific sequence, were executed independently, and the corresponding NTS was computed. The DD sequence exhibiting the lowest NTS was chosen for each problem size n . Thus, our final results, discussed below, compare the unprotected ‘no-DD’ circuits with DD-protected circuits where the NTS was minimized for each n separately over all the sequences in \mathcal{D} .

The results for all the sequences in \mathcal{D} , in support of our DD sequence ranking methodology, are presented in Appendix K.

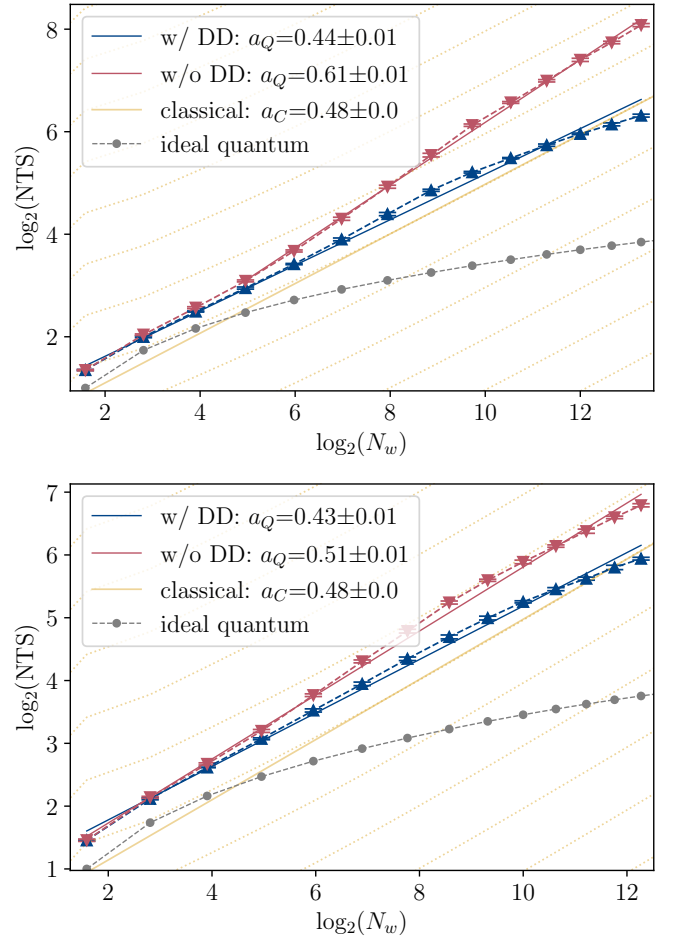


FIG. 3. NTS as a function of $\log_2(N_w)$ on Sherbrooke (top) for w_6 Simon-15 and Brisbane (bottom) for w_5 Simon-15, both with MEM. The red lines represent the unprotected, no-DD form of the algorithm. The blue lines represent the DD-protected form, i.e., a circuit where DD fills the idle gaps, with the optimal DD sequence from \mathcal{D} used at each problem size n . The dashed lines connect the data points and the solid lines are least-squares fits. The function in Eq. (13) is fitted for n in the range $[2, 15]$ for both Sherbrooke and Brisbane. Uncertainties expressed using “ \pm ” in the legend are the 95% confidence intervals. The error bars, representing confidence intervals derived through bootstrapping, extend 5σ in both directions from each data point. The yellow solid line represents $\text{NTS}_C^{\text{lb}}(N_w)$, the lower bound on the classical NTS [Eq. (7)]. The yellow dotted lines with the same slope as the asymptotic slope of the solid yellow line are a guide to the eye. The grey dashed line is the theoretical performance of the quantum algorithm running on a noiseless device, given by Eq. (11).

VI. RESULTS AND DISCUSSION

Our first main result is shown in Fig. 3, which plots the NTS as a function of problem size n for the w_6 Simon-15 (w_5 Simon-15) problem run on the 127-qubit Sherbrooke (Brisbane) device. The measurement results were post-processed using MEM before attempting to solve for b ; see Appendix L for details. We used bootstrapping to compute

all means and standard deviations, as documented in Appendix M. We found Sherbrooke to be the top-performing device for solving Simon’s problem. The main difference between Sherbrooke and Brisbane pertinent to the somewhat better performance of Sherbrooke in our experiments is its much smaller 2-qubit gate error: a mean of 0.02% vs. 1%, respectively (see Appendix J).

The fitted values a_x where $x \in \{Q, C\}$ as given in Eq. (13) are shown in the legend. In order to present the least biased result for the quantum scaling, we report the *worst*-case slope a_Q . We determine this value as follows: we fit Eq. (13) for $n_{\min} \leq n \leq n_{\max}$ with $n_{\min} \in [2, n_{\max} - 1]$ and report the highest value of a_Q . We find $n_{\min} = 2$ in the DD-protected case for both Sherbrooke and Brisbane; see Appendix N for details. We set $n_{\max} = 15$ since the results for $n > 15$ are essentially random, as shown in Appendix O (additionally, MEM becomes impractical for $n > 15$ due to time and memory costs). From Fig. 3, we observe that $a_Q = 0.44 \pm 0.01$ for w_6 Simon-15 run on Sherbrooke and $a_Q = 0.43 \pm 0.01$ for w_5 Simon-15 run on Brisbane, both subject to DD protection, where the uncertainty represents 95% confidence intervals. We therefore declare a subexponential algorithmic quantum speedup for the DD-protected w_w Simon- n problem for $w = 6$ on Sherbrooke and $w = 5$ on Brisbane.

Whether there is further evidence of an algorithmic quantum speedup is determined by comparing a_C and a_Q over a range of w values. This brings us to our second main result, shown in Fig. 4, where we plot a_C and a_Q with and without DD, as a function of w . Numerical fitting of the form displayed in Fig. 3 but extended to other values of w shows that a_C quickly approaches approximately 0.5, as expected from the classical NTS and as remarked below Eq. (7). As is further clear from Fig. 4, the algorithmic quantum speedup persists for the DD-protected w_w Simon- n problem for $w \leq 6$ on Sherbrooke and $w \leq 5$ on Brisbane. The speedup becomes ambiguous at $w = 7$ ($w = 6$) on Sherbrooke (Brisbane) and disappears for $w \geq 8$ ($w \geq 7$). Without DD, we observe a speedup on both devices only for $w \leq 4$.

Further analysis shows that the speedup does not extend to $w > 7$ on Sherbrooke or to $w > 6$ on Brisbane, even with DD protection. Additional results for the 27-qubit devices Cairo and Kolkata are shown in Appendix P, for which we do not find evidence of a speedup.

The speedup we find for the w_w Simon-15 problem involves 30 physical qubits. The previously reported algorithmic quantum speedup result for the single-shot Bernstein-Vazirani problem extended to 27 physical qubits and used the 27-qubit Montreal processor [41]. Our present result thus increases both the number of physical qubits for which an algorithmic quantum speedup has been reported and the complexity of the quantum algorithm for which the result holds.

VII. SUMMARY AND CONCLUSIONS

The goal of demonstrating an algorithmic quantum speedup, i.e., a quantum speedup that scales favorably as the problem size grows, is central to establishing the utility of

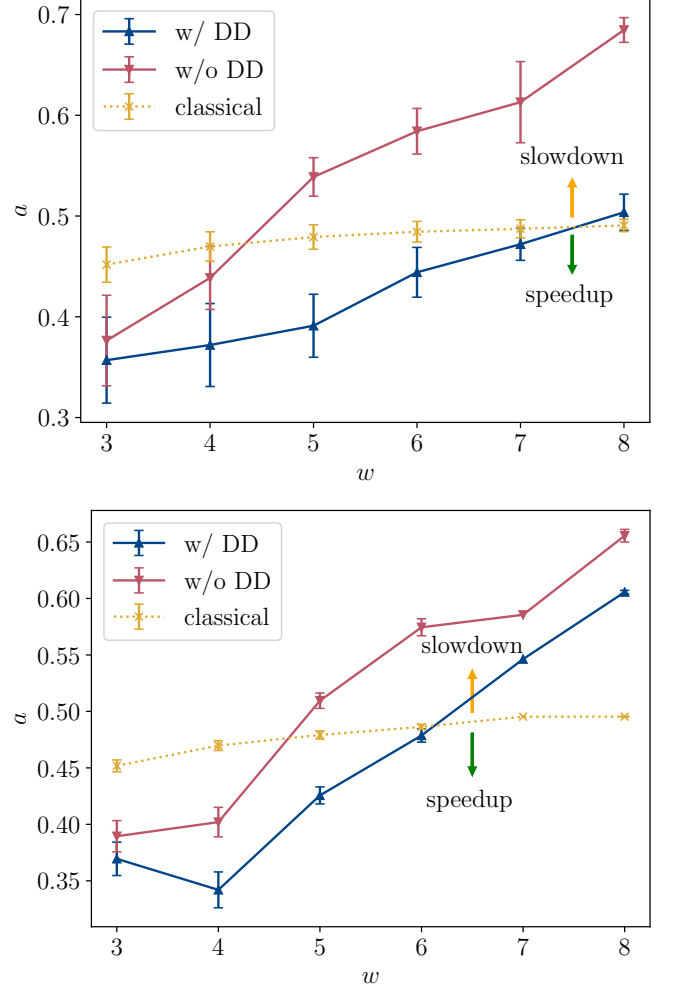


FIG. 4. The fitted scaling parameter a as a function of w for w_w Simon-15 on Sherbrooke (top) and Brisbane (bottom), both with MEM. When the quantum slope is below the classical slope, we declare an algorithmic quantum speedup. This holds with statistical confidence for $w \leq 6$ ($w \leq 5$) on Sherbrooke (Brisbane). The error bars, representing the standard deviation of the fitted parameter a on the bootstrapped data, extend 1σ in each direction from each data point.

quantum computers. Simon’s problem is an early example of the Abelian hidden subgroup problem and a precursor to Shor’s factoring algorithm. It requires exponential time to solve on a classical computer but only linear time on a noiseless quantum computer, assuming we count oracle queries but do not account for the actual resources spent on executing the oracle. Here, we studied a modified version of Simon’s problem, which restricts the allowed Hamming weight of the hidden bitstring to $w \leq n$. The classical solution of this version scales as $n^{w/2}$. Our goal was to determine whether NISQ devices are capable of providing an algorithmic quantum speedup in solving this version of Simon’s problem.

We ran restricted-HW Simon’s algorithm experiments on the IBM Quantum platform and demonstrated that two 127-qubit devices, Sherbrooke and Brisbane, exhibit an algorith-

mic quantum speedup, which extended to larger HW values when we incorporated suitably optimized DD protection. MEM further enhanced the speedup.

These results significantly extend the scope of conjecture-free algorithmic quantum speedups for oracular algorithms. More generally, our work expands the frontier of empirical quantum advantage results and suggests that algorithmic quantum speedup results involving practically relevant algorithms may also be within reach.

VIII. ACKNOWLEDGEMENTS

We thank Bibek Pokharel for useful discussions. This research was supported by the ARO MURI grant W911NF-22-S-0007 and is based in part upon work supported by the National Science Foundation the Quantum Leap Big Idea under Grant No. OMA-1936388. This material is also based upon work supported by the Defense Advanced Research Projects Agency (DARPA) under Contract No. HR001122C0063. ZZ and GQ acknowledge funding from the U.S. Department of Energy (DOE), Office of Science, Office of Advanced Scientific Computing Research (ASCR), Accelerated Research in Quantum Computing program under Award Number DE-SC0020316. This research used resources of the Oak Ridge Leadership Computing Facility, which is a DOE Office of Science User Facility supported under Contract DE-AC05-00OR22725.

Appendix A: Compiler

We explained in Section II A that even for a fixed b the choice of f requires at least $(n-1)2^{n-1}$ encoding bits, leading to infeasibly deep circuits for NISQ devices. To circumvent this problem, we introduce the notion of a compiler that performs the following functions: (i) it hides the implementation details of f from the player; (ii) it takes a circuit C with 0 or more boxes labeled “ \mathcal{O} ” and produces a circuit C' obtained from C by replacing each \mathcal{O} box with a circuit implementing it for the current f ; (iii) further compiles C' to ensure that it is compatible with the gate set and connectivity of the NISQ device, to reduce the number of gates and the circuit depth, and to select the best layout of the qubits on the device (i.e., avoiding the noisiest qubits and couplings), yielding a new circuit C'' and classical post-processing instructions; (iv) sends C'' to the NISQ device for execution, obtains the result, performs the post-processing, and returns the final result to the player. Note that in (ii), “ \mathcal{O} ” is just a box labeling a place to insert the oracle (which is unknown to the player), as opposed to \mathcal{O}_f , which is the unitary implementing the actual oracle.

When defining these rules, we need to be careful about the optimizations allowed in step (iii): if we allow too few, the circuit C'' may be too large to be executed with reasonable fidelity; if we allow too many, C'' may become a no-op and all computations will be performed by classical post-processing.

To understand the rules we choose, consider the intended circuit C and the circuit \mathcal{O}_f implementing the

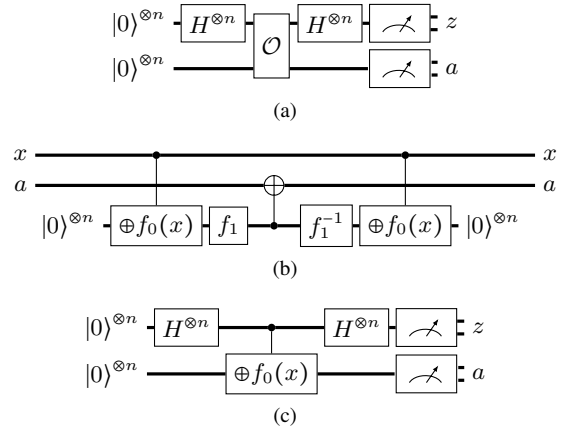


FIG. 5. (a) The intended circuit C . The thick wires indicate that each wire represents $n > 1$ qubits. H denotes a Hadamard gate and \mathcal{O} denotes the oracle. (b) Circuit implementing the oracle \mathcal{O}_f for arbitrary f satisfying the conditions (i)–(iii). Any such f can be decomposed as $f(x) = f_1(f_0(x))$, where f_0 is any 2-to-1 function satisfying condition (ii) with the same b , and f_1 is a permutation of bitstrings. All gates are classical in the sense that if the input $|x, a\rangle$ consists of a single computational basis state (with amplitude 1), so does the output. The circuit for f_1 may need 3-qubit gates and ancillary qubits. The unitary controlled- $(\oplus f_0(x))$ maps a computational basis element $|x\rangle|a\rangle$ to $|x\rangle|a \oplus f_0(x)\rangle$. The gate sequence shown is one possible implementation of \mathcal{O}_f : the circuit prepares $f(x)$ on a third n -qubit register, performs a CNOT with the a register as the target, and uncomputes the third register to return it to the $|0\rangle$ state. (c) Compiled circuit. This circuit is equivalent to the unoptimized circuit shown in (a) and (b), assuming f_1 is applied to a in post-processing (such optimization is allowed by the rules).

oracle, shown in Fig. 5(a) and Fig. 5(b), respectively. To see why Fig. 5(b) implements the oracle, note first that any f satisfying conditions (i)–(iii) can be written as $f(x) = f_1(f_0(x))$. To verify the circuit, it suffices to ensure that it works as intended on computational basis states, i.e., it maps $|x\rangle|a\rangle$ to $|x\rangle|a \oplus f_1(f_0(x))\rangle$. As is easily verified, the list of states along the computation is $|x\rangle|a\rangle \mapsto |x\rangle|a\rangle|0\rangle^{\otimes n} \mapsto |x\rangle|a\rangle|f_0(x)\rangle \mapsto |x\rangle|a\rangle|f_1(f_0(x))\rangle \mapsto |x\rangle|a \oplus f_1(f_0(x))\rangle|f_1(f_0(x))\rangle \mapsto |x\rangle|a \oplus f_1(f_0(x))\rangle|f_0(x)\rangle \mapsto |x\rangle|a \oplus f_1(f_0(x))\rangle|0\rangle^{\otimes n} \mapsto |x\rangle|a \oplus f_1(f_0(x))\rangle$, as required.

Before formulating the rules below, we introduce the notion of classical gates. We say that a gate is classical if it maps computational basis states (with amplitude 1) to computational basis states. In particular, X , CNOT, and the Toffoli (CCNOT) are classical, but Y , Z , and H are not. Performing a classical gate immediately before the measurement in the computational basis is equivalent to performing the measurement first and then applying the equivalent classical post-processing.

Based on this, we state the following rules for the compiler: (1) it can perform a joint optimization of C' , that is, it does not have to preserve the separation between the gates inside and outside \mathcal{O}_f ; (2) it can perform any optimization that does not change the output distribution of C' if it were executed on an ideal quantum computer; (3) it can replace classi-

cal gates before the measurement with the equivalent classical post-processing; (4) rules #2 and #3 can be applied any number of times in any order.

With these rules, we expect the compiler to be able to compile the circuit in Fig. 5(a) with \mathcal{O}_f from Fig. 5(b) into the circuit C'' as shown in Fig. 5(c). Moreover, we expect that the qubits of the x and a registers will be reordered such that circuits with the same $HW(b)$ will be compiled into the same circuit. The application of f_1 and the inverse of the qubit reordering will be done by classical post-processing. Note that Fig. 1 is an expanded version of Fig. 5.

Appendix B: Simon's oracle construction

Although the structure of the oracle is not known to the player who wishes to solve Simon's problem, someone needs to play the role of the 'verifier' who acts like a referee, that is, construct the oracle for the player and verify whether the player's guess is correct. The verifier needs to know the structure of the quantum oracle f_b in order to construct the quantum circuit for each hidden bitstring b . Since it is a Clifford circuit, the oracle presented below can be efficiently simulated by a classical computer. However, this does not destroy the claimed speedup because our setting assumes the 'black box' scenario [57], i.e., the players are not allowed to know the structure of the oracle and solve the problem in linear time by classically constructing the oracle on their own.

Before presenting it, we remark that our oracle construction is not unique; it only needs to satisfy the condition specified by Simon's problem, i.e., $\forall x, y \in \{0, 1\}^n$, $f_b(x) = f_b(y)$ if and only if $x = y$ or $x = y \oplus b$ for a hidden bitstring $b \in \{0, 1\}^n$.

To aid in visualization, we will interchangeably use quantum circuits and directed graphs to represent the oracle. This is useful because the oracle circuit consists entirely of CNOT gates, which can be represented as arrows from the controlled qubit to the target qubit. Fig. 6 shows an example of how to transform between the two representations. The data (d_j) and ancilla (a_j) qubits are drawn in the first and second columns in the graph representation, respectively.

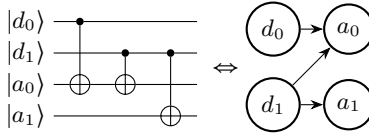


FIG. 6. Conversion between a pure-CNOT circuit and its graph representation. A CNOT gate is an arrow from the controlled to the target qubit.

Two operations are used to construct the oracle: classical copy and classical addition modulo 2. Both are classical operations executed by quantum devices.

- Classical copy: This operation copies a classical state from a 1-qubit register into another 1-qubit register. Fig. 7 shows an example of copying $|d_0d_1\rangle$ into the ancilla qubits $|a_0a_1\rangle$, which are initialized as $|00\rangle$.

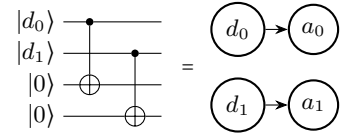


FIG. 7. A quantum circuit for the operation $|d_0d_1\rangle|00\rangle \mapsto |d_0d_1\rangle|d_0d_1\rangle$. $d_0, d_1, a_0, a_1 \in \{0, 1\}$.

- Classical XOR: This operation performs the XOR (single-digit addition modulo 2) between two 1-qubit registers and stores the result in another 1-qubit register. Fig. 8 shows an example of adding $|d_0d_1\rangle$ and storing the result in the first ancilla qubit $|a_0\rangle$, which is initialized as $|0\rangle$.

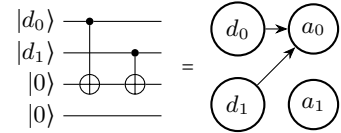


FIG. 8. A quantum circuit that applies the operation $|d_0d_1\rangle|00\rangle \mapsto |d_0d_1\rangle|d_0 \oplus d_1, 0\rangle$. $d_0, d_1, a_0, a_1 \in \{0, 1\}$.

Next, we show how to construct a 2-to-1 oracle. We represent a length- n bitstring $x = x_0 \dots x_{n-1}$, where $x_j \in \{0, 1\}$, and use an oracle that transforms $|x\rangle|0\rangle \mapsto |x\rangle|f_b(x)\rangle$ when $b = 0^{n-i}1^i$. For each b of this form, $f_b : \{0, 1\}^n \mapsto \{0, 1\}^n$ is defined as follows:

$$f_b(x) = (x_0, \dots, x_{n-i-1}, 0, x_{n-i+1} \oplus x_{n-i}, \dots, x_{n-1} \oplus x_{n-i}) \quad (B1)$$

for $1 \leq i \leq n$.

Equivalently, we can write this transformation as

$$|x_0 \dots x_{n-1}\rangle_d |0^n\rangle_a \mapsto |x_0 \dots x_{n-1}\rangle_d |x_0 \dots x_{n-i-1} 0 (x_{n-i} \oplus x_{n-i+1}) \dots (x_{n-i} \oplus x_{n-1})\rangle_a. \quad (B2)$$

The following Lemmas show that $f_b(x)$ is a valid family of oracles for Simon's problem.

Lemma 1. $f_b(x) = f_b(y)$ if and only if $x = y$ or $y = x \oplus b$, where $b = 0^{n-i}1^i$, $1 \leq i \leq n$. I.e., $f_b(x)$ is a 2-to-1 function.

Proof. Consider two ancilla registers containing the output from two different inputs x and y . According to Eq. (B2), we can write $f_b(x)$ and $f_b(y)$ as

$$\begin{aligned} |f_b(x)\rangle &= |x_0 \dots x_{n-i-1} 0 (x_{n-i} \oplus x_{n-i+1}) \dots (x_{n-i} \oplus x_{n-1})\rangle \\ |f_b(y)\rangle &= |y_0 \dots y_{n-i-1} 0 (y_{n-i} \oplus y_{n-i+1}) \dots (y_{n-i} \oplus y_{n-1})\rangle. \end{aligned} \quad (B3)$$

(\Rightarrow) If $x = y$ or $y = x \oplus b$, then $f_b(x) = f_b(y)$: The statement is trivial when $x = y$. We explicitly write $b = 0_0 \dots 0_{n-i-1} 1_{n-i} \dots 1_{n-1}$, so that $\{y_0 \dots y_{n-i-1}\} = \{x_0 \dots x_{n-i-1}\}$ and $\{y_{n-i+1} \dots y_{n-1}\} = \{x_{n-i+1} \oplus 1 \dots x_{n-1} \oplus 1\}$. It follows from Eq. (B1) that trivially $f_b(y_j) = f_b(x_j)$ for $j \leq n-i$ and that for $j \geq n-i+1$, $f_b(y_j) = y_{n-i} \oplus y_j = (x_{n-i} \oplus 1) \oplus (x_j \oplus 1) = x_{n-i} \oplus x_j = f_b(x_j)$.

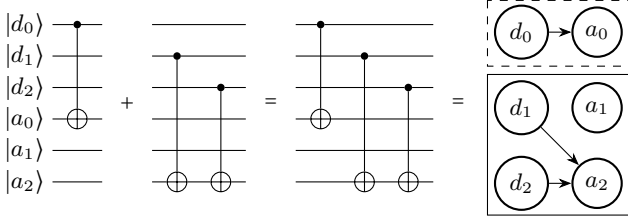


FIG. 9. Construction of an oracle for solving the Simon-3 problem with $b = 011$ according to Eq. (B2). The first (second) part in the dashed (solid) box applies classical copy (XOR), corresponding to the 0's (1's) in b .

(\Leftarrow) If $f_b(x) = f_b(y)$, then $x = y$ or $y = x \oplus b$: The calculation in the ' \Rightarrow ' part of the proof shows that $f_b(y) = f_b(x)$ if $y = x \oplus b$; therefore, $f_b^{-1}(x)$ outputs x and $x \oplus b$ and likewise, $f_b^{-1}(y)$ outputs y and $y \oplus b$. Hence, $f_b(x) = f_b(y)$ implies that either (1) $x = y$ and $x \oplus b = y \oplus b$, or (2) $x = y \oplus b$ and $x \oplus b = y$. Case (1) corresponds to $x = y$ and case (2) corresponds to $y = x \oplus b$.

The conclusion that $f_b(x)$ is a 2-to-1 function now follows directly. \square

Having shown that f_b as defined in Eq. (B1) and written explicitly in Eq. (B2) is a valid oracle for Simon's problem, we proceed to construct its quantum version using classical copy (for the first $n - i$ positions) and classical XOR (for the last i positions). The a_{n-i} qubit remains in the $|0\rangle$ state, hence no operation is required.

To construct the first $n - i$ positions in Eq. (B2), one needs to copy the state in d_0, \dots, d_{n-i-1} into a_0, \dots, a_{n-i-1} . The quantum operation for this is a CNOT from each qubit d_j of the data register (controlled qubit) to the corresponding qubit a_j in the ancilla register (target qubit), as shown in Fig. 7.

To construct the last i positions in Eq. (B2), one needs to perform XOR on d_{n-i} and d_j from the data register and store the result in the qubit a_j in the ancilla register. Two CNOTs are required from two controlled qubits, d_{n-i} and d_j , onto the same target qubit a_j , similarly to what is shown in Fig. 8.

We can construct an oracle for a Simon- n problem using this method. Where to apply classical copy or classical XOR depends on the hidden bitstring $b = 0^{n-i}1^i$: a 0 is an instruction to copy, while a 1 is an instruction to perform an XOR. Fig. 9 shows an example of combining these two types of operators to construct an oracle for Simon-3 with $b = 011$. Fig. 10 shows an example of Simon-5 in the graph representation. An example of the full quantum circuit to solve a Simon-3 problem with $b = 011$ is given in Fig. 11.

Appendix C: Alternative derivation of the classical complexity of Simon's problem

An alternative derivation of the classical complexity of Simon's problem can be given in the spirit of the birthday paradox. Given any input bitstring pair $x_i \neq x_j$ such that $f_b(x_i) = f_b(x_j)$ (a collision), we have the solution to Simon's problem: $b = x_i \oplus x_j$. In the worst case, excluding

the 0^n string, it takes $k_{\max} = 2^{n-1}$ strings to find a collision. But suppose we pick $k < k_{\max}$ strings at random. There are $\binom{k}{2} = k(k-1)/2$ pairs. Given a random string x_i , we can pick a second random string x_j , and $x_j \neq 0^n, x_i$ with probability $1/(N_n - 1)$, where $N_n = 2^n - 1$. This is also the probability of a collision between x_i and x_j . Therefore

$$\Pr[f_b(x_i) = f_b(x_j)] = \frac{\binom{k}{2}}{N_n - 1}, \quad i \neq j. \quad (\text{C1})$$

Setting $\Pr[f_b(x_i) = f_b(x_j)] = 1$ guarantees a collision. Solving for k , the required number of queries k in Eq. (C1) is $O(2^{n/2})$.

The classical complexity is affected by the change of the total number of possible b 's from N_n to $N_w = \sum_{j=1}^w \binom{n}{j}$ in w Simon- n . Hence, Eq. (C1) becomes:

$$\Pr[f_b(x_i) = f_b(x_j)] = \frac{\binom{k}{2}}{N_w - 1}. \quad (\text{C2})$$

By setting $\Pr[f_b(x_i) = f_b(x_j)] \geq 1$, we assume that a collision is not found until all bitstring pairs have been tested, which yields the worst-case number of classical queries (for the best possible classical algorithm), and we recover Eq. (5).

Appendix D: Upper bound on NTS_C

As remarked in the main text, there is no guarantee that the player will find a sequence of bitstrings $x = \{x_1, x_2, \dots, x_k\}$ that achieves the lower bound on NTS_C given by Eq. (7). For Eq. (6) to be an equality, all values of $x_l \oplus x_m$ should be different and satisfy $\text{HW}(x_l \oplus x_m) \leq w$ for $1 \leq l < m \leq k$. To find an upper bound on NTS_C , we consider an arbitrary sequence x_1, \dots, x_k of bitstrings that a classical player intends to submit to the oracle. Without loss of generality, we can assume that this sequence is independent of the oracle replies unless a match $f(x_j) = f(x_l)$ is found for $j < l \leq k$ (in which case the classical player stops and returns $b = x_j \oplus x_l$). We can also assume that

$$|S \setminus S_j| \leq 1 \Leftrightarrow j = k. \quad (\text{D1})$$

If Eq. (D1) is not satisfied for $j = k$, the classical algorithm fails to find b for $b \in S \setminus S_k$, and if Eq. (D1) is satisfied for $j < k$, we can set k to the smallest such j . Equation (D1) can be seen as an exact version of Eq. (5): it ensures that k is the worst-case classical number of queries of an algorithm described by the sequence x . For x satisfying Eq. (D1), we can compute the NTS exactly:

$$\text{NTS}_C(x) = \sum_{i=0}^{k-1} \left(\frac{|S \setminus S_i|}{|S|} \right) = \sum_{i=0}^{k-1} \left(1 - \frac{|S_i|}{|S|} \right), \quad (\text{D2})$$

which is the exact version of Eq. (6). Then

$$\text{NTS}_C = \min_{x: \text{Eq. (D1)}} \text{NTS}_C(x). \quad (\text{D3})$$

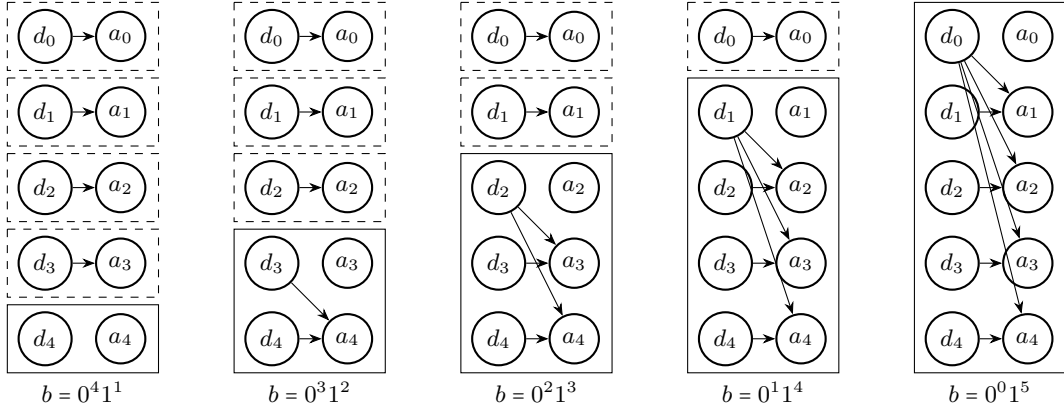


FIG. 10. Oracle construction for Simon-5 in the graph representation. Using the reduction procedure, we can remove the dashed boxes to arrive at Simon- m , where $m < 5$.

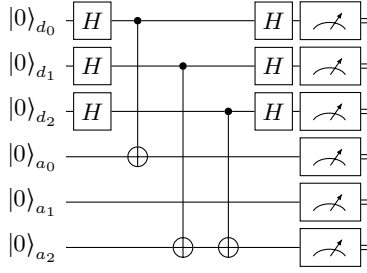


FIG. 11. The quantum circuit to solve the Simon-3 problem with $b = 011$, which can be extracted from the dashed (d_2, a_2) box and the lowermost solid box in Simon-5 with $b = 0^3 1^2$.

We do not know a method to find this minimum exactly for $n \geq 10$ because, as n grows, the search space involves sequences of k bitstrings, where k grows exponentially with n , i.e., the search space size grows as $2^{n2^{n/2}}$ for the original Simon's problem and as $2^n \sqrt{\binom{n}{w}}$ for w_w Simon- n with constant w , which is infeasible already for $n = 10$, $w = 6$. We circumvent this problem using a heuristic search for larger n . If we could show that the sequence x we found using a heuristic search minimizes Eq. (D3), then we would be able to claim that we found the exact value of NTS_C . In practice, we cannot show this for all but the few smallest values of n , hence we can only claim that $\text{NTS}_C \leq \text{NTS}_C(x)$.

The solution we compute for Eq. (D3) from a heuristic search serves as the upper bound for NTS_C , while Eq. (7) represents its lower bound. We selected the latter when contrasting the slope parameters a_Q and a_C . This ensures that the quantum algorithm's performance surpasses the lower threshold of its classical counterpart, guaranteeing a quantum scaling advantage if achieved.

In larger problem sizes where the upper and lower bounds do not align, the actual NTS_C lies somewhere between the two. The discrepancy between the theoretical lower bound in Eq. (7) and the heuristic upper bound in Eq. (D3) is depicted in Fig. 12 for w_5 Simon- n and w_6 Simon- n from $n = 2$ to $n = 15$.

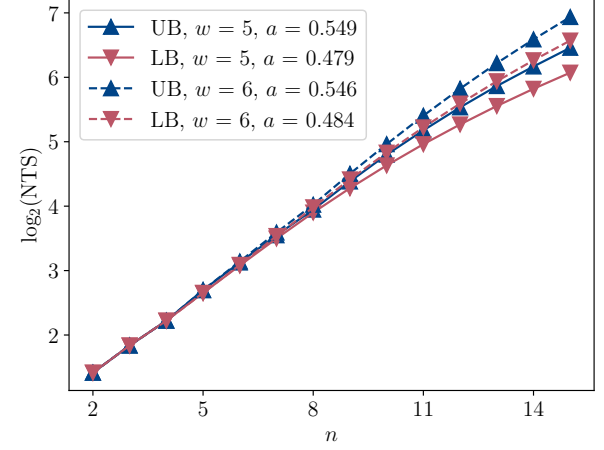


FIG. 12. Difference between the upper bound (UB) and lower bound (LB) of NTS_C and the corresponding slope parameter a for $w = 5$ and $w = 6$. We use the LB slope in the quantum speedup analysis.

Appendix E: Solving Simon- n in $O(n)$ oracle queries on a noiseless QC

We prove that the circuit in Fig. 1 solves Simon's problem in $O(n)$ oracle queries, assuming that it is run on a noiseless QC. Starting from the left of Fig. 1, every qubit is initialized in the all-zero state $|\psi_0\rangle = |0\rangle^{\otimes n} |0\rangle^{\otimes n}$, and the first n Hadamard gates put every data qubit into a uniform superposition:

$$|\psi_1\rangle = H^{\otimes n} |\psi_0\rangle = \frac{1}{\sqrt{2^n}} \sum_{x \in \{0,1\}^n} |x\rangle |0\rangle^{\otimes n}. \quad (\text{E1})$$

Next, for an input x , the oracle \mathcal{O}_b outputs $f_b(x)$ stored in the ancilla register, where $f_b(x) = f_b(y)$ if and only if $y = x$ or $y = x \oplus b$,

$$|\psi_2\rangle = \mathcal{O}_b |\psi_1\rangle = \frac{1}{\sqrt{2^n}} \sum_{x \in \{0,1\}^n} |x\rangle |f_b(x)\rangle. \quad (\text{E2})$$

The ancilla qubits are then measured in the computational basis, an operation denoted by $M_a^{\otimes n}$. The result could be any $f_b(x)$ where $x \in \{0, 1\}^n$ with equal probability, which is then discarded. The remaining state in the data register is

$$|\psi_3\rangle = M_a^{\otimes n} |\psi_2\rangle = \frac{1}{\sqrt{2}}(|x\rangle + |x \oplus b\rangle). \quad (\text{E3})$$

Applying the last set of Hadamard gates on the data qubits, we have

$$|\psi_b\rangle = H^{\otimes n} |\psi_3\rangle \quad (\text{E4a})$$

$$= \frac{1}{\sqrt{2^{n+1}}} \sum_{z \in \{0, 1\}^n} [(-1)^{x \cdot z} + (-1)^{(x \oplus b) \cdot z}] |z\rangle \quad (\text{E4b})$$

$$= \frac{1}{\sqrt{2^{n-1}}} \sum_{\{z|z \cdot b = 0\}} (-1)^{x \cdot z} |z\rangle, \quad (\text{E4c})$$

where the last line arises from the fact that the element in the sum vanishes when $x \cdot z \neq (x \oplus b) \cdot z$. The remaining terms must have $x \cdot z = (x \oplus b) \cdot z$, which reduces to $z \cdot b = 0, \forall x$.

Appendix F: Proof of Theorem 1

Proof. The $|S| = 1$ case is trivial. To prove the lower bound in Eq. (8), consider the situation after k executions of the circuit. It is known that b is uniformly distributed in some subset S_k of S (e.g., $S_0 = S$). Let B_k be the random variable representing the value of b and Z_k be the random variable representing the value of z obtained from the $k+1$ 'th execution of the circuit. Then the information gain about B_k from Z_k is given by their mutual information $I(B_k; Z_k) = H(B_k) + H(Z_k) - H(B_k, Z_k)$, where H is the Shannon entropy. We have $H(B_k) = \log_2 |S_k|$, $H(Z_k) \leq n$, and $H(B_k, Z_k) = (n-1) + \log_2 |S_k|$ [because (B_k, Z_k) is uniformly distributed across $|S_k| 2^{n-1}$ pairs (b, z) : for each b there are 2^{n-1} options for z (the ones satisfying $b \cdot z = 0$)]. Hence $I(B_k; Z_k) \leq 1$, and it follows that $\text{NTS}_{\text{IQ}} \geq \log_2 |S|$: we learn at most 1 bit of information in every step and we need to learn $\log_2 |S|$ bits.

To prove the upper bound in Eq. (8), let b^* be the true (hidden) value of b and let $S^* = S \setminus \{b^*\}$. For each $b \in S^*$ let X_b be the random variable representing the number of circuit executions needed to learn that $b^* \neq b$. Since upon each circuit execution z is uniformly distributed among all z s.t. $z \cdot b^* = 0$, we know that X_b is geometrically distributed: $\Pr(X_b = k) = 2^{-k}$ for $k \geq 1$. Let $X_{\max} = \max_{b \in S^*} X_b$. Then

$$\Pr(X_{\max} = k) \leq \sum_{b \in S^*} \Pr(X_b = k) = (|S| - 1) 2^{-k}, \quad (\text{F1})$$

which implies $\Pr(X_{\max} \geq k) \leq (|S| - 1) 2^{1-k}$. Now, let $a = \lfloor \log_2 (|S| - 1) \rfloor$ and let b be the fractional part of $\log_2 (|S| - 1)$

so that $|S| - 1 = 2^{a+b}$. We have:

$$\begin{aligned} \text{NTS}_{\text{IQ}} &= \mathbb{E}[X_{\max}] = \sum_{k=1}^{\infty} \Pr(X_{\max} \geq k) \\ &\leq \sum_{k=1}^{\infty} \min(1, 2^{a+b+1-k}) = \sum_{k=1}^{a+1} 1 + \sum_{k=a+2}^{\infty} 2^{a+b+1-k} \\ &= a + 1 + 2^b = \log_2 (|S| - 1) + 1 + 2^b - b \\ &\leq \log_2 (|S| - 1) + 2, \end{aligned} \quad (\text{F2})$$

where in the second line we used $\sum_{k'=k}^{\infty} 2^{-k'} = 2^{1-k}$.

Equation (9) follows from the observation that in the first step we either obtain $z = 0^n$ with probability 2^{1-n} , in which case we learn nothing about b^* , or we reduce the problem to Simon- $(n-1)$. Each term in the sum in Eq. (9) represents the expected number of steps needed to reduce the problem Simon- $(k+1)$ to Simon- k . The Erdős-Borwein constant is defined as $E_{\text{EB}} \equiv \sum_{k=1}^{\infty} 1/(2^k - 1)$, so $\sum_{k=1}^{n-1} \frac{1}{1-2^{-k}} - (n + E_{\text{EB}} - 1) = -\sum_{k=n}^{\infty} 1/(2^k - 1) = O(2^{-n})$.

Equation (10) follows from the observation that for $w = 1$ all X_b are independent, hence the task of computing NTS_{IQ} reduces to the task of computing the expected value of the maximum of $n-1$ independent geometrically distributed random variables, which was solved in [58]. \square

Appendix G: Ideal quantum NTS_{IQ} calculation

Theorem 1 states the upper and lower bounds for NTS_{IQ} and that it can be calculated exactly for the two limiting cases $w = 1$ and $w = \infty$. In the main text, we constructed an interpolation between the two known values, Eqs. (9) and (10), which we can rewrite as:

$$\text{NTS}_{\text{IQ}} = \log_2 (N_w) + t\Gamma_{w=\infty} + (1-t)\Gamma_{w=1}, \quad (\text{G1})$$

where the weighted $\Gamma_{w=\infty} = E_{\text{EB}} - 1$ and $\Gamma_{w=1} = 0.5 + \gamma/\ln(2)$ are constants from Eqs. (9) and (10), respectively.

An alternative approach is to use a Monte Carlo simulation to compute NTS_{IQ} . For a w Simon- n problem, we randomly picked $10 b^*$'s from the possible set S_0 such that $|S_0| = N_w$. For each b^* , a series of valid z_k 's such that $b^* \cdot z_k = 0$ is drawn. After each z_k was drawn, we eliminated any b in S_k that did not satisfy $b \cdot z_k = 0$ and stopped when $|S_k| = 1$. At this point, we expected to only have b^* as the only element left in S_k . The simulated NTS_{IQ} was calculated 10,000 times for each b^* , and the average was taken. After performing the simulation for 10 b^* 's, we found the mean and standard deviation and reported this as the Monte Carlo version of NTS_{IQ} .

Fig. 13 compares the upper bound and lower bound from Eq. (8), the interpolated version of NTS_{IQ} , and the Monte Carlo version of NTS_{IQ} for $w = 5$ and 6.

Appendix H: Post-processing for the ‘NISQ’ variant of the quantum algorithm

The original noiseless solver requires sampling $n-1$ independent output bitstrings z 's and solves for the unique b that

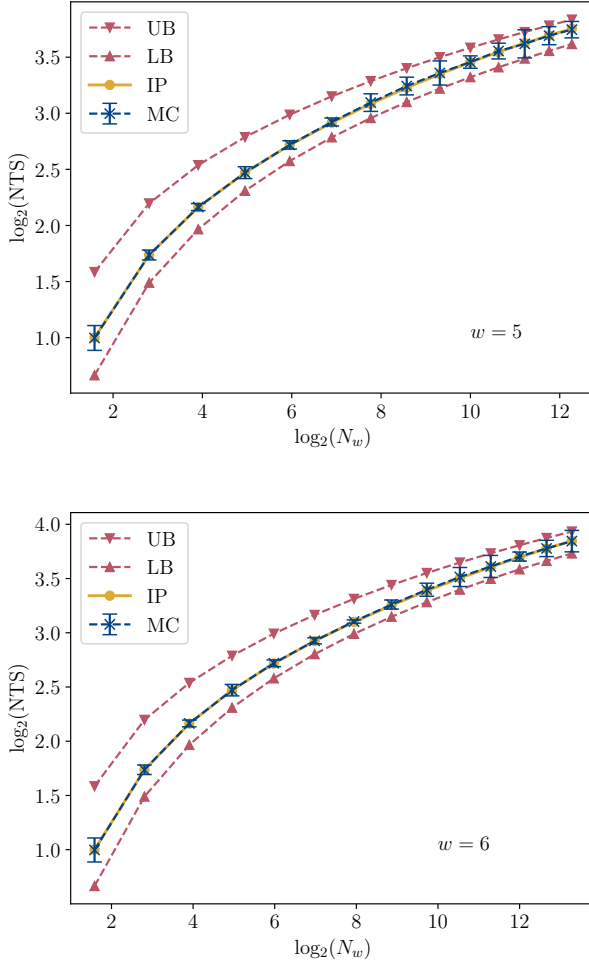


FIG. 13. Upper bound (UB) and lower bound (LB) from Eq. (8), the interpolated version of NTSIQ (IP), and the Monte Carlo version of NTSIQ (MC) for $w = 5$ (top) and 6 (bottom). The error bars on the blue lines are 5σ in each direction.

satisfies $z \cdot b = 0, \forall z$. This means that if one of the z 's is altered by noise, the resulting b is guaranteed to be wrong. To reduce the effect of noise, we employ Algorithm 1, a post-processing algorithm that applies in the ‘NISQ’ setting described in the main text.

Algorithm 1 requires $K = O(kn)$ queries, but since $k = O(1)$, the quantum speedup is maintained under the NTS metric, i.e., the algorithm’s query complexity remains $O(n)$.

We find that optimal NTS performance is achieved when $k = 2$ across a majority of problem sizes. The variable K extracted from the algorithm specified in Algorithm 1 represents the actual count of shots (queries) utilized in solving for b . This quantity is denoted Q_i in Eq. (12), where $i = \text{HW}(b)$.

Data: input $n, K_{\min} \in \mathbb{N}$, stream Z of bitstrings
 Initialize a dictionary B : $B[b'] = 0, \forall b' \in \{0, 1\}^n, b' \neq 0$;
 Initialize $K = 0$;
while $K < K_{\min}$ or $\text{argmax}(B)$ is not unique **do**
 $K = K + 1$;
 $z = \text{next}(Z)$;
for b' in $\text{keys}(B)$ **do**
if $z \cdot b' = 0$ **then**
 $B[b'] = B[b'] + 1$;
end
end
end
return $b' = \text{argmax}(B)$ and K ;

Algorithm 1: Solving for b in $K \geq K_{\min}$ shots

Appendix I: Circuit Complexity Reduction

To avoid the impractical task of running $2^n - 1$ different oracles for every possible hidden bitstring for Simon- n problems, we use permutation symmetry and only run n circuits for a problem size n . Our chosen bitstrings are $b^i = 0^{n-i}1^i$ for $1 \leq i \leq n$. The number of queries Q_i for each b^i is weighted in the NTS calculation in Eq. (12) according to the corresponding weight $h_i = \binom{n}{i}$, as explained in Section IV. We assume that the permutation symmetry and weighting are processed within the compiler, as detailed in Appendix A.

We aim to quantify the quantum speedup for a fixed $w \leq n$. To further reduce the number of circuits, instead of running w_w Simon- n for every n and w , we only run w_w Simon- n_{\max} and extract the w_w Simon- m cases where $m < n_{\max}$ during post-processing.

Furthermore, we reduce Simon- n to Simon- m , where $m < n$. For example, we can use the result of the experiment at problem size $n = 15$ to extract the results for smaller problem sizes, $m = 2$ to $m = 14$. Figure 14 shows an example of the reduction from $n = 3$ ($b = 011$) to $m = 2$ ($b = 11$).

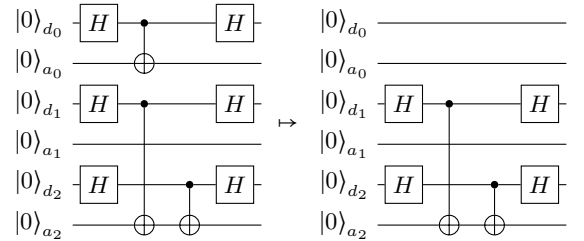


FIG. 14. Circuit reduction from Simon-3 to Simon-2. The right circuit $m = 2$ ($b = 11$) can be extracted from the left circuit $n = 3$ ($b = 011$) by tracing out qubits d_0 and a_0 .

This reduction is possible under the assumption of a CPTP map governing the circuit in the open-system setting. We give the proof of this fact next.

Since qubits (d_j, a_j) are unentangled in our oracle construction from the rest of the circuit if the j th bit of the hidden bitstring b is zero, these two qubits are separated from the rest of the oracle, as indicated by the individual dashed boxes in Fig. 10. Therefore, the only difference between

$b_n = 0^{n-i}1^i$ and $b_m = 0^{m-i}1^i$ is that the circuit for $|b_n| = n$ applies extra operations on extra qubits compared to the circuit for $|b_m| = m$. Let $m \in [i, n-1]$; then all the circuits for $b_m = 0^{m-i}1^i$ have the identical output as the circuit for $b_n = 0^{n-i}1^i$ if we consider only the overlapping set of qubits, as illustrated in Fig. 14. Intuitively, we may thus extract the Simon- m results from the Simon- n results by running only the Simon- n circuits and tracing over the first $2(n-m)$ data qubits, a practice we implemented in our experiments and subsequent analysis. Note that the left circuit in Fig. 14 is the same circuit as in Fig. 11 but drawn with a different qubit order.

Let us now prove the equivalence of our procedure to actually running the Simon- m circuits, as long as the completely positive, trace preserving (CPTP) map governing the circuit in the open system case factors into a product over the “copied” and “XOR-ed” qubits, i.e., those corresponding to a 0 (copied) or 1 (XOR-ed) in the bitstring b that defines the given oracle.

In preparation for our more general discussion below, let us equivalently represent the action of the closed-system Simon- n circuit with hidden bitstring b on some initial state ρ of the n data and n ancilla qubits as

$$\text{Simon}_n(b)[\rho] = \text{Tr}_a [(H_d^{\otimes n} \circ \mathcal{O}_b \circ H_d^{\otimes n})[\rho]], \quad (I1)$$

where \mathcal{O}_b represents the Simon oracle, and Tr_a means that the state of the ancilla qubits (labeled a_0, \dots, a_{n-1}) is discarded at the end, so that $\text{Simon}_n(b)[\rho]$ is the state of the n data qubits at the end of one run of the algorithm. Thus, if we write $\Pi_b = |\psi_b\rangle\langle\psi_b|$ and $|\psi_0\rangle\langle\psi_0| = \Pi_{0^n} \otimes \Pi_{0^n}$, then it follows from Eq. (I1) that $\text{Simon}_n(b)[|\psi_0\rangle\langle\psi_0|] = \Pi_b$.

Let us denote the qubit sets as follows: $D_\nu = \{d_0, \dots, d_{n-m-1}\}$ ($A_\nu = \{a_0, \dots, a_{n-m-1}\}$) being the first $n-m$ data (ancilla) qubits and $D_\mu = \{d_{n-m}, \dots, d_{n-1}\}$ ($A_\mu = \{a_{n-m}, \dots, a_{n-1}\}$) being the remaining m data (ancilla) qubits in the circuit. Let $\cup_\nu \equiv D_\nu \cup A_\nu = \{d_0, a_0, \dots, d_{n-m-1}, a_{n-m-1}\}$. Let us show that if $b_n = 0^{n-i}1^i$, then

$$\text{Simon}_m(b_m)[\Pi_{0^m} \otimes \Pi_{0^m}] = \text{Tr}_{\cup_\nu} [\text{Simon}_n(b_n)[|\psi_0\rangle\langle\psi_0|]], \quad (I2)$$

where the trace means that the states of qubits in \cup_ν are discarded from the result of running $\text{Simon}_n(b_n)$. To prove this claim in the absence of any noise, note that:

$$\text{Tr}_{\cup_\nu} [\text{Simon}_n(b_n)[|\psi_0\rangle\langle\psi_0|]] \quad (I3a)$$

$$= \text{Tr}_{\cup_\nu} [\Pi_{b_n}] \quad (I3b)$$

$$= \text{Tr}_{\cup_\nu} [\Pi_\nu \otimes \Pi_{b_m}] \quad (I3c)$$

$$= \Pi_{b_m} \quad (I3d)$$

$$= \text{Simon}_m(b_m)[\Pi_{0^m} \otimes \Pi_{0^m}], \quad (I3e)$$

as claimed. Here, $b_n = 0^{n-i}1^i$, $b_m = 0^{m-i}1^i$ ($m < n$) and in the third line, $\Pi_\nu = |\psi_\nu\rangle\langle\psi_\nu|$, where $|\psi_\nu\rangle = |+\rangle^{n-m}$ is derived

from the last line of Eq. (I1):

$$\frac{1}{\sqrt{2^{n-1}}} \sum_{\{z|z \cdot b_n = 0\}} (-1)^{x \cdot z} |z\rangle_d \quad (I4a)$$

$$= \frac{1}{\sqrt{2^{n-1}}} \sum_{y \in \{0,1\}^{n-m}} |y\rangle_{D_\nu} \otimes \sum_{\{z|z \cdot b_m = 0\}} (-1)^{x \cdot z} |z\rangle_{D_\mu} \quad (I4b)$$

$$= \frac{1}{\sqrt{2^{n-m}}} \sum_{y \in \{0,1\}^{n-m}} |y\rangle_{D_\nu} \otimes \frac{1}{\sqrt{2^{m-1}}} \sum_{\{z|z \cdot b_m = 0\}} (-1)^{x \cdot z} |z\rangle_{D_\mu} \quad (I4c)$$

$$= |\psi_\nu\rangle \otimes |\psi_{b_m}\rangle. \quad (I4d)$$

Now consider the case where each gate is represented not by a unitary but by a CPTP map. We can rewrite the initial state as

$$|\psi_0\rangle\langle\psi_0| = \Pi_{0^n} \otimes \Pi_{0^n} = \rho_\nu \otimes \rho_\mu, \quad (I5)$$

where $\rho_\nu = \Pi_{0^{n-m}} \otimes \Pi_{0^{n-m}}$ and $\rho_\mu = \Pi_{0^m} \otimes \Pi_{0^m}$. The Simon oracle does not introduce any two-qubit gates between qubit sectors $\cup_\mu = D_\mu \cup A_\mu$ and $\cup_\nu = D_\nu \cup A_\nu$, so it is reasonable to assume that under the coupling to the environment, they remain uncoupled (as long as there is no unintended crosstalk between the two sectors). Therefore, the CPTP map for the noisy Simon- n algorithm will be

$$\mathcal{S}_n(b_n)[\rho_\nu \otimes \rho_\mu] = \text{Tr}_{\cup_\nu} [(\mathcal{H}_\nu \otimes \mathcal{H}_\mu) \circ (\mathcal{O}_\nu \otimes \mathcal{O}_\mu) \circ (\mathcal{H}_\nu \otimes \mathcal{H}_\mu)[\rho_\nu \otimes \rho_\mu]], \quad (I6)$$

where $\mathcal{H}_{\nu,\mu}$ and $\mathcal{O}_{\nu,\mu}$ represent the CPTP maps corresponding to the experimental implementation of the unitaries H (multi-qubit Hadamard) and \mathcal{O}_f (oracle) acting on qubit sectors ν, μ . Recall that for arbitrary CPTP maps \mathcal{U} and \mathcal{V} acting on a tensor-product space

$$\mathcal{U} \otimes \mathcal{V}[\rho \otimes \sigma] = \mathcal{U}[\rho] \otimes \mathcal{V}[\sigma]. \quad (I7)$$

Therefore,

$$\text{Tr}_{\cup_\nu} [\mathcal{S}_n(b_n)[|\psi_0\rangle\langle\psi_0|]] \quad (I8a)$$

$$= \text{Tr}_{\cup_\nu} [(\mathcal{H}_\nu \otimes \mathcal{H}_\mu) \circ (\mathcal{O}_\nu \otimes \mathcal{O}_\mu) \circ (\mathcal{H}_\nu \otimes \mathcal{H}_\mu)[\rho_\nu \otimes \rho_\mu]] \quad (I8b)$$

$$= \text{Tr}_{\cup_\nu} [(\mathcal{H}_\nu \circ \mathcal{O}_\nu \circ \mathcal{H}_\nu)[\rho_\nu] \otimes (\mathcal{H}_\mu \circ \mathcal{O}_\mu \circ \mathcal{H}_\mu)[\rho_\mu]] \quad (I8c)$$

$$= \mathcal{S}_m(b_m)[\rho_\mu] \quad (I8d)$$

$$= \mathcal{S}_m(b_m)[\Pi_{0^m} \otimes \Pi_{0^m}]. \quad (I8e)$$

This is the CPTP map generalization of the closed-system result Eq. (I2), and it shows that the reduction from Simon- n to Simon- m holds rigorously also in the open system setting, as long as the CPTP map factors according to the qubit sectors ν and μ .

Appendix J: Device specifications

We performed our experiments on two 127-qubit and two 27-qubit IBM Quantum devices, respectively: Brisbane and

Sherbrooke, and Cairo and Kolkata. Table I and Table II give the device specifications.

We used 100,000 shots per experiment parameterized by the Hamming weight of the oracle b for each device.

	Brisbane			Sherbrooke		
	Min	Mean	Max	Min	Mean	Max
$T_1(\mu s)$	27.59	290.03	519.75	45.60	233.38	404.29
$T_2(\mu s)$	11.21	173.18	439.99	9.45	144.76	366.50
1QG Error (%)	0.026	0.080	0.424	0.028	0.118	3.324
2QG Error (%)	0.278	0.376	100	0.373	2.437	100
1QG Duration (μs)	0.171	0.171	0.171	0.180	0.180	0.180
2QG Duration (μs)	0.448	0.539	0.882	0.660	0.665	0.860
RO Error (%)	0.180	1.813	27.670	0.430	2.063	11.90
RO Duration (μs)	1.244	1.244	1.244	4.000	4.000	4.000

TABLE I. Device specifications for the 127-qubit devices Brisbane and Sherbrooke on May 5, 2023. 1QG and 2QG denote 1-qubit gate and 2-qubit gate, respectively. RO denotes readout. The numbers shown are averages over the qubits used in our experiments.

	Cairo			Kolkata		
	Min	Mean	Max	Min	Mean	Max
$T_1(\mu s)$	63.79	116.39	195.17	37.13	121.03	235.27
$T_2(\mu s)$	15.59	97.63	212.26	16.35	74.51	192.35
1QG Error (%)	0.043	0.093	0.356	0.047	0.090	0.204
2QG Error (%)	0.491	4.680	100	0.591	11.98	100
1QG Duration (μs)	0.075	0.075	0.075	0.107	0.107	0.107
2QG Duration (μs)	0.160	0.351	0.946	0.341	0.458	0.626
RO Error (%)	0.750	1.679	6.120	0.340	2.607	11.76
RO Duration (μs)	0.732	0.732	0.732	0.640	0.640	0.640

TABLE II. Device specifications for the 27-qubit devices Cairo and Kolkata on April 20 and 22, 2023, respectively. 1QG and 2QG denote 1-qubit gate and 2-qubit gate, respectively. RO denotes readout. The numbers shown are averages over the qubits used in our experiments.

Appendix K: DD performance

This section presents the performance evaluation of all DD sequences investigated in the experiments on Sherbrooke and Brisbane, specifically the 12 sequences from the set \mathcal{D} as introduced in Section V. The performance assessed by the NTS metric is illustrated in Fig. 15. The NTS values are presented for each DD sequence across the problem size n , in the range $[2, 15]$. Sequences colored in blue (\times) indicate optimal performers identified on their corresponding machines at each problem size. The analysis reveals that UR₁₀ (RGA8a) exhibits the best performance among sequences on Sherbrooke (Brisbane), consistently achieving the lowest NTS across a majority of n ranging from 7 to 15.

Appendix L: Error Mitigation

DD suppresses noise during circuit execution. To complement DD, we used measurement error mitigation (MEM) [59] as a means to reduce measurement-related errors in the NISQ algorithm setting. Information on device properties was collected on the days our experiments were run and used as correction matrices in PyIBU [60], which runs MEM based on iterative Bayesian unfolding.

Fig. 16 shows the probability of obtaining $z \cdot b = 0$ as a function of n , the length of the hidden bitstring b . An improvement resulting from the application of MEM is visible.

Appendix M: Bootstrapping

We conducted a robust statistical analysis employing a 100,000-sample bootstrapping technique on the NTS values subjected to a 10-fold cross-validation. Each sample, consisting of 9 uniformly selected data points from the cross-validation set, underwent resampling to derive the mean and standard deviation. The resulting bootstrapped means and standard deviations are presented as individual data points in Fig. 3 and Fig. 15, where the mean values are plotted as data points, with error bars extending 5σ in both directions. These statistics are then used to fit for the parameter a using Scipy’s `curve_fit`, also reported as the “ \pm ” uncertainties in Fig. 3, taking into account the bootstrapped mean as the NTS value and one standard deviation as its error. In Fig. 4 and Fig. 17, the parameter a was fitted using the bootstrapped data in the same way as in Fig. 3 but with different w values. The standard deviation from the fitting is reported as 1σ in each direction from each data point.

Appendix N: Determination of n_{\min}

Figure 18 shows that $n_{\min} = 2$ in the DD-protected case for both Sherbrooke and Brisbane. In the unprotected case, we see that $n_{\min} = 5$ and $n_{\min} = 2$ for Sherbrooke and Brisbane, respectively.

Maximizing the confidence intervals on a_Q until they overlap a_C , we find that $a_C > a_Q$ with 99.4% and 99.9% confidence on Sherbrooke and Brisbane, respectively, as can also be seen from Fig. 18.

Appendix O: Mutual information

Solving Simon’s problem requires a series of “good” outcomes of the form $z \cdot b = 0$ and $z \neq 0$. Let p be the probability of $z \cdot b = 0$ and let q be the probability of obtaining $z = 0$. The result of each measurement round then falls into one of the following three categories:

$$\begin{aligned} \Pr(z = 0) &= q, \\ \Pr(z \cdot b = 0 | z \neq 0) &= (1 - q)p, \\ \Pr(z \cdot b = 1 | z \neq 0) &= (1 - q)(1 - p). \end{aligned} \quad (O1)$$

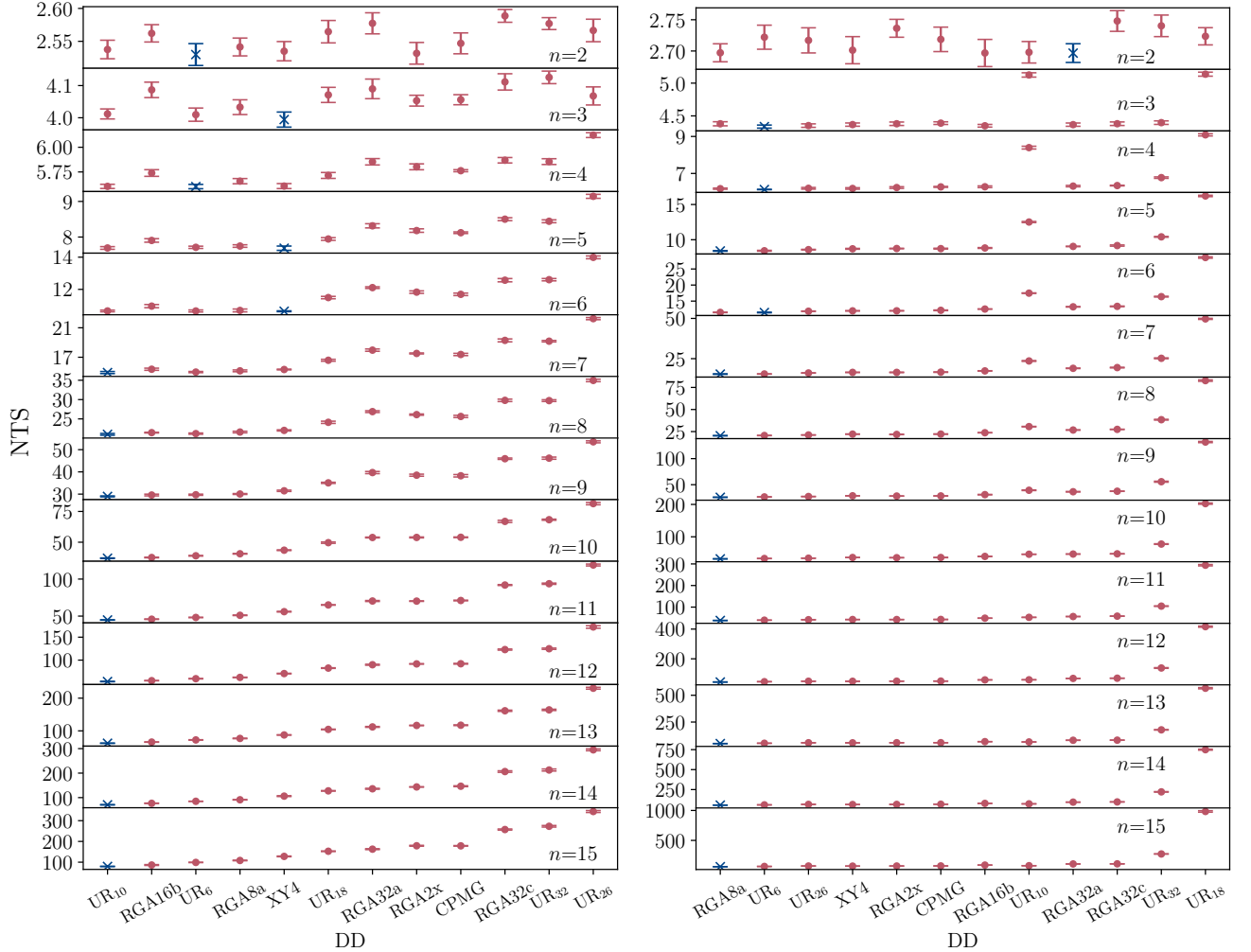


FIG. 15. DD performance under NTS metric on Sherbrooke (left) and Brisbane (right) over the 12 sequences in the set $\mathcal{D} = \{\text{CPMG}, \text{RGA}_{2x}, \text{XY4}, \text{UR}_6, \text{RGA}_{8a}, \text{UR}_{10}, \text{RGA}_{16b}, \text{UR}_{18}, \text{UR}_{26}, \text{RGA}_{32a}, \text{RGA}_{32c}, \text{UR}_{32}\}$. Sequences colored in blue (\times) denote those identified as optimal performers on their respective machines at varying problem sizes n . The arrangement of sequences in the plot reflects their performance averaged over all problem sizes n . UR_{10} and RGA_{8a} emerge as the best-performing sequence overall on Sherbrooke and Brisbane, respectively, and become the top-performing sequences for all $n \geq 7$ on both devices. The error bars, representing confidence intervals derived through bootstrapping, extend 5σ in both directions from each data point.

We can extract p and q from the counts data of the experiment. The probability $\Pr(z \cdot b = 0) = q + (1 - q)p$ for both 127-qubit devices is plotted in Fig. 16. Note that we set $p = 0$ when $n = 1$ by definition. This is because the only possible non-zero hidden bitstring is $b = 1$ when $n = 1$, hence, every z such that $z \cdot b = 0$ is $z = 0$, which contributes only to q . With this choice, we start the plot in Fig. 16 from $n = 2$.

We calculate the estimated information gained per circuit round, with the optimistic assumption that we gain the same amount of information in every round. Letting $S(X)$ denote the Shannon entropy of a random variable X , the classical

mutual information $I(Z; B)$ is defined as

$$\begin{aligned}
 I(Z; B) &= S(Z) + S(B) - S(Z|B) \\
 &= \sum_{z,b} \Pr(z, b) \log_2 \frac{\Pr(z, b)}{\Pr(z)\Pr(b)} \\
 &= \sum_{z,b} \Pr(z|b)\Pr(b) \log_2 \frac{\Pr(z|b)}{\Pr(z)} \\
 &= \left(\sum_b \Pr(b) \right) \left(\sum_z \Pr(z|b) \log_2 \frac{\Pr(z|b)}{\Pr(z)} \right) \\
 &= \sum_z \Pr(z|b) \log_2 \frac{\Pr(z|b)}{\Pr(z)}.
 \end{aligned} \tag{O2}$$

To go from the second to the third line, we used the fact that $\Pr(z|b)\Pr(b) = \Pr(z, b)$. In the fourth line, the summation over b is separated from the summation over z because the

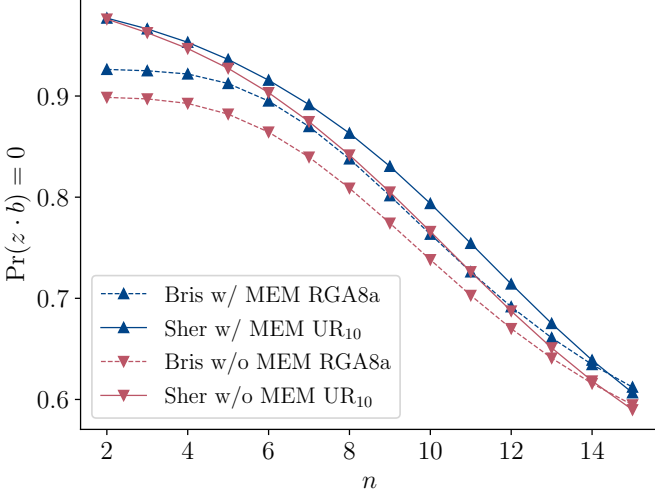


FIG. 16. Probability of obtaining $z \cdot b = 0$ with and without MEM on Brisbane (Bris) and Sherbrooke (Sher). The data shown uses the best-performing DD sequences on each device.

quantity in the second bracket is independent of b by permutation symmetry. We used $\sum_b \Pr(b) = 1$ to arrive at the last line and remove the dependence on b .

Consider dividing the sum into three cases according to Eq. (O1), we have $I(Z; B) = \sum_{i=1,2,3} I^i(Z; B)$, where $I^i(Z; B)$ is given as follows.

- Case I: $z = 0$.

$$\begin{aligned} I^1(Z; B) &= \Pr(z = 0|b) \log_2 \frac{\Pr(z = 0|b)}{\Pr(z = 0)} \\ &= q \log_2 \frac{q}{q} = 0. \end{aligned} \quad (\text{O3})$$

- Case II: $z \cdot b = 0, z \neq 0$. There are $N_2 = 2^{n-1} - 1$ possibilities of z 's (half of 2^n and excluding 0).

$$\begin{aligned} I^2(Z; B) &= \sum_z \Pr(z \cdot b = 0 \wedge z \neq 0|b) \log_2 \frac{\Pr(z \cdot b = 0 \wedge z \neq 0|b)}{\Pr(z \cdot b = 0 \wedge z \neq 0)} \\ &= \sum_z \frac{(1-q)p}{N_2} \log_2 \frac{(1-q)p/N_2}{(1-q)/(2^n - 1)} \\ &= (1-q)p \log_2 \frac{p(2^n - 1)}{2^{n-1} - 1} \end{aligned} \quad (\text{O4})$$

- Case III: $z \cdot b = 1, z \neq 0$. There are $N_3 = 2^{n-1}$ possibilities of z 's (half of 2^n).

$$\begin{aligned} I^3(Z; B) &= \sum_z \Pr(z \cdot b = 1 \wedge z \neq 0|b) \log_2 \frac{\Pr(z \cdot b = 1 \wedge z \neq 0|b)}{\Pr(z \cdot b = 1 \wedge z \neq 0)} \\ &= \sum_z \frac{(1-q)(1-p)}{N_3} \log_2 \frac{(1-q)(1-p)/N_3}{(1-q)/(2^n - 1)} \\ &= (1-q)(1-p) \log_2 \frac{(1-p)(2^n - 1)}{2^{n-1}} \end{aligned} \quad (\text{O5})$$

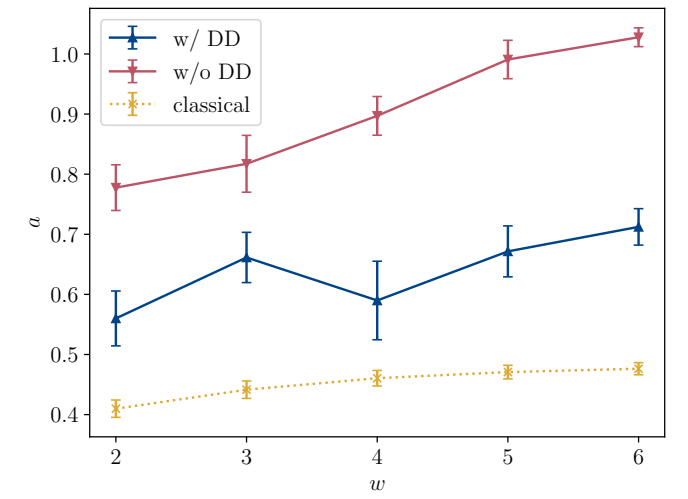
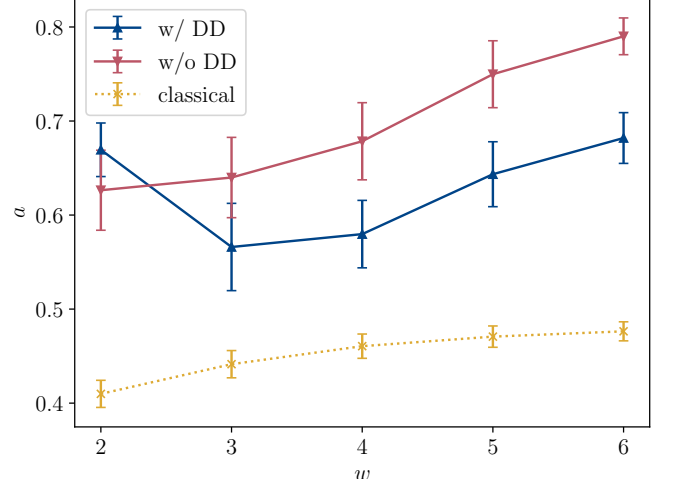


FIG. 17. The fitted scaling parameter a as a function of w for w_w Simon-13 on Cairo (top) and Kolkata (bottom), both with MEM. When the quantum slope is below the classical slope, we declare an algorithmic quantum speedup. This does not hold for any value of w , and instead, we observe a quantum slowdown, even with DD. The error bars, representing the standard deviation of the fitted parameter a on the bootstrapped data, extend 1σ in each direction from each data point.

We can calculate the classical mutual information $I(Z; B)$ in terms of p and q as the sum of Eq. (O3), Eq. (O4), and Eq. (O5):

$$\begin{aligned} I(Z; B) &= (1-q) \left(p \log_2 \frac{p(2^n - 1)}{2^{n-1} - 1} \right. \\ &\quad \left. + (1-p) \log_2 \frac{(1-p)(2^n - 1)}{2^{n-1}} \right). \end{aligned} \quad (\text{O6})$$

The expected information learned per circuit, $I(Z; B)$, is plotted as a function of problem size n in Fig. 19. We compare the free evolution and the top-performing DD sequence of each device with and without MEM. From this information, we expect, on average, to see these top-performing sequences having better scaling in the NTS metric.

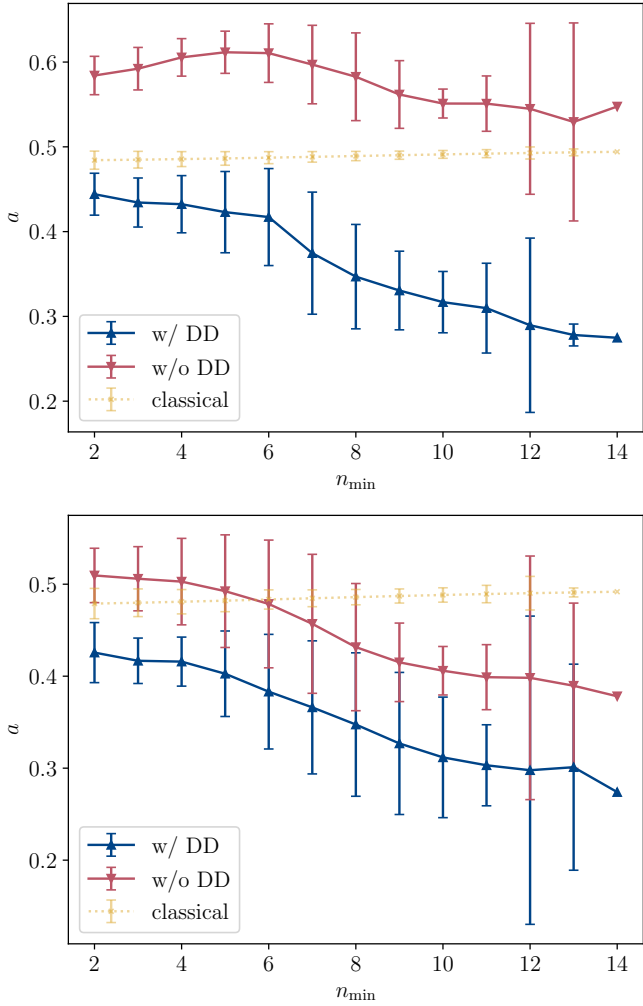


FIG. 18. The fitted scaling parameter a as a function of n_{\min} on Sherbrooke for w_6 Simon-15 (top) and Brisbane for w_5 Simon-15 (bottom), both with MEM. The error bars represent 99.4% (99.9%) confidence intervals on Sherbrooke (Brisbane), except for $n_{\min} = 13$, where we show an error bar of 10σ . This choice arises from the t -value used for calculating the confidence interval at $n_{\min} = 13$, which is approximately 10 times larger than that of other n_{\min} values. There is no error bar for $n_{\min} = 14$ because only two points are involved in the curve fitting. We report the a value that is maximized over the range of n_{\min} shown. In the unprotected case, this corresponds to $n_{\min} = 5$ on Sherbrooke and $n_{\min} = 2$ on Brisbane. In the DD-protected case, all values of a lie below the classical value, but we report the worst-case result obtained for $n_{\min} = 2$ on both devices.

Both Figs. 16 and 19 confirm that the results are essentially random for $n > 15$, as stated in the main text.

Appendix P: Results for 27-qubit devices: no evidence of an algorithmic quantum speedup

We performed the same set of experiments on two 27-qubit IBM Quantum devices, Cairo (ibm_cairo) and Kolkata

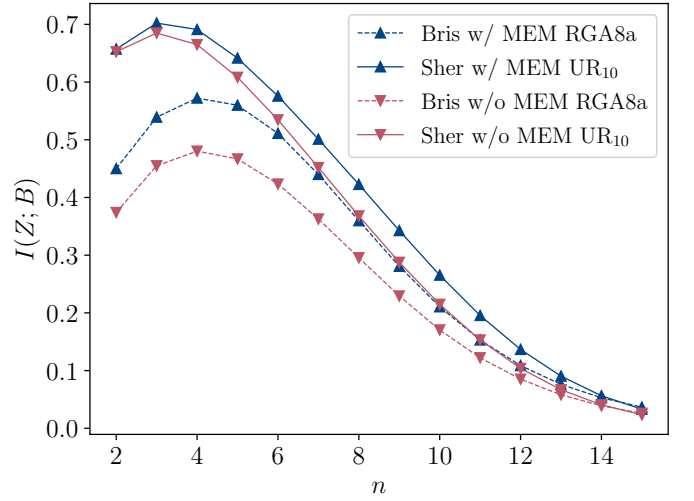


FIG. 19. Information learned per circuit with and without MEM from the best sequence on 127-qubit devices, Brisbane (BB) and Sherbrooke (SB).

(ibmq_kolkata), each with 100,000 shots. Both devices feature the heavy-hex lattice and the Falcon r5.11 processor. Their specifications at the time of our experiments are given in Table II.

For these experiments, we set $n_{\max} = 13$, the maximum possible value compatible with 27 qubits. Unlike the 127-qubit devices discussed in the main text, there is no evidence of quantum speedup for any Hamming weight considered, as seen from Fig. 17 (contrast with Fig. 4). However, DD protection still results in a significant improvement.

[1] David Deutsch and Richard Jozsa, “Rapid solution of problems by quantum computation,” *Proceedings of the Royal Society of London. Series A: Mathematical and Physical Sciences, Proceedings of the Royal Society of London. Series A: Mathematical and Physical Sciences* **439**, 553–558 (1992).

[2] Ethan Bernstein and Umesh Vazirani, “Quantum Complexity Theory,” *SIAM J. Comput.* **26**, 1411–1473 (1997).

[3] Daniel R. Simon, “On the power of quantum computation,” *SIAM Journal on Computing* **26**, 1474–1483 (1997).

[4] Lov K. Grover, “Quantum mechanics helps in searching for a needle in a haystack,” *Phys. Rev. Lett.* **79**, 325–328 (1997).

[5] P. Shor, “Polynomial-time algorithms for prime factorization and discrete logarithms on a quantum computer,” *SIAM Journal on Computing* **26**, 1484–1509 (1997).

[6] Andrew M Childs, Richard Cleve, Enrico Deotto, Edward Farhi, Sam Gutmann, and Daniel A Spielman, “Exponential algorithmic speedup by a quantum walk,” in *Proceedings of the thirty-fifth annual ACM symposium on Theory of computing* (ACM, 2003) pp. 59–68.

[7] Wim Van Dam, Sean Hallgren, and Lawrence Ip, “Quantum algorithms for some hidden shift problems,” *SIAM Journal on Computing* **36**, 763–778 (2006).

[8] Aram W. Harrow, Avinatan Hassidim, and Seth Lloyd, “Quantum algorithm for linear systems of equations,” *Physical Review Letters* **103**, 150502– (2009).

[9] Ashley Montanaro, “Quantum algorithms: An overview,” *NPJ Quantum Inf.* **2**, 15023 (2016).

[10] Sergey Bravyi, David Gosset, and Robert König, “Quantum advantage with shallow circuits,” *Science* **362**, 308 (2018).

[11] Sergey Bravyi, David Gosset, Robert König, and Marco Tomamichel, “Quantum advantage with noisy shallow circuits,” *Nature Physics* **16**, 1040–1045 (2020).

[12] Kishor Bharti, Alba Cervera-Lierta, Thi Ha Kyaw, Tobias Haug, Sumner Alperin-Lea, Abhinav Anand, Matthias Degroote, Hermanni Heimonen, Jakob S. Kottmann, Tim Menke, Wai-Keong Mok, Sukin Sim, Leong-Chuan Kwek, and Alán Aspuru-Guzik, “Noisy intermediate-scale quantum algorithms,” *Reviews of Modern Physics* **94**, 015004– (2022).

[13] Andrew J. Daley, Immanuel Bloch, Christian Kokail, Stuart Flannigan, Natalie Pearson, Matthias Troyer, and Peter Zoller, “Practical quantum advantage in quantum simulation,” *Nature* **607**, 667–676 (2022).

[14] John Preskill, “Quantum Computing in the NISQ era and beyond,” *Quantum* **2**, 79 (2018).

[15] Tameem Albash and Daniel A. Lidar, “Demonstration of a scaling advantage for a quantum annealer over simulated annealing,” *Physical Review X* **8**, 031016– (2018).

[16] Andrew D. King, Jack Raymond, Trevor Lanting, Sergei V. Isakov, Masoud Mohseni, Gabriel Poulin-Lamarre, Sara Ejtemaei, William Bernoudy, Isil Ozfidan, Anatoly Yu. Smirnov, Mauricio Reis, Fabio Altomare, Michael Babcock, Catia Baron, Andrew J. Berkley, Kelly Boothby, Paul I. Bunyk, Holly Christami, Colin Enderud, Bram Evert, Richard Harris, Emile Hoskinson, Shuiyuan Huang, Kais Jooya, Ali Khodabandehloou, Nicolas Ladizinsky, Ryan Li, P. Aaron Lott, Allison J. R. MacDonald, Danica Marsden, Gaelen Marsden, Teresa Medina, Reza Molavi, Richard Neufeld, Mana Norouzpour, Travis Oh, Igor Pavlov, Ilya Perminov, Thomas Prescott, Chris Rich, Yuki Sato, Benjamin Sheldon, George Sterling, Loren J. Swenson, Nicholas Tsai, Mark H. Volkmann, Jed D. Whittaker, Warren Wilkinson, Jason Yao, Hartmut Neven, Jeremy P. Hilton, Eric Ladizinsky, Mark W. Johnson, and Mohammad H. Amin, “Scaling advantage over path-integral monte carlo in quantum simulation of geometrically frustrated magnets,” *Nature Communications* **12**, 1113 (2021).

[17] V. Saggio, B. E. Asenbeck, A. Hamann, T. Strömberg, P. Schianky, V. Dunjko, N. Friis, N. C. Harris, M. Hochberg, D. Englund, S. Wölk, H. J. Briegel, and P. Walther, “Experimental quantum speed-up in reinforcement learning agents,” *Nature* **591**, 229–233 (2021).

[18] Federico Centrone, Niraj Kumar, Eleni Diamanti, and Iordanis Kerenidis, “Experimental demonstration of quantum advantage for np verification with limited information,” *Nature Communications* **12**, 850 (2021).

[19] Dmitri Maslov, Jin-Sung Kim, Sergey Bravyi, Theodore J. Yoder, and Sarah Sheldon, “Quantum advantage for computations with limited space,” *Nature Physics* **17**, 894–897 (2021).

[20] Yi Xia, Wei Li, Quntao Zhuang, and Zheshen Zhang, “Quantum-enhanced data classification with a variational entangled sensor network,” *Physical Review X* **11**, 021047– (2021).

[21] Hsin-Yuan Huang, Michael Broughton, Jordan Cotler, Sitan Chen, Jerry Li, Masoud Mohseni, Hartmut Neven, Ryan Babbush, Richard Kueng, John Preskill, and Jarrod R. McClean, “Quantum advantage in learning from experiments,” *Science* **376**, 1182–1186 (2022).

[22] S. Ebadi, A. Keesling, M. Cain, T. T. Wang, H. Levine, D. Bluvstein, G. Semeghini, A. Omran, J.-G. Liu, R. Samajdar, X.-Z. Luo, B. Nash, X. Gao, B. Barak, E. Farhi, S. Sachdev, N. Gemelke, L. Zhou, S. Choi, H. Pichler, S.-T. Wang, M. Greiner, V. Vuletic, and M. D. Lukin, “Quantum optimization of maximum independent set using rydberg atom arrays,” *Science* **376**, 1209–1215 (2022).

[23] Min-Gang Zhou, Xiao-Yu Cao, Yu-Shuo Lu, Yang Wang, Yu Bao, Zhao-Ying Jia, Yao Fu, Hua-Lei Yin, and Zeng-Bing Chen, “Experimental Quantum Advantage with Quantum Coupon Collector,” *Research* **2022** (2022).

[24] Andrew D. King, Jack Raymond, Trevor Lanting, Richard Harris, Alex Zucca, Fabio Altomare, Andrew J. Berkley, Kelly Boothby, Sara Ejtemaei, Colin Enderud, Emile Hoskinson, Shuiyuan Huang, Eric Ladizinsky, Allison J. R. MacDonald, Gaelen Marsden, Reza Molavi, Travis Oh, Gabriel Poulin-Lamarre, Mauricio Reis, Chris Rich, Yuki Sato, Nicholas Tsai, Mark Volkmann, Jed D. Whittaker, Jason Yao, Anders W. Sandvik, and Mohammad H. Amin, “Quantum critical dynamics in a 5,000-qubit programmable spin glass,” *Nature* **617**, 61–66 (2023).

[25] Youngseok Kim, Andrew Eddins, Sajant Anand, Ken Xuan Wei, Ewout van den Berg, Sami Rosenblatt, Hasan Nayfeh, Yantao Wu, Michael Zaletel, Kristan Temme, and Abhinav Kandala, “Evidence for the utility of quantum computing before fault tolerance,” *Nature* **618**, 500–505 (2023).

[26] Scott Aaronson and Lijie Chen, “Complexity-theoretic foundations of quantum supremacy experiments,” in *Proceedings of the 32nd Computational Complexity Conference*, CCC ’17 (Schloss Dagstuhl–Leibniz-Zentrum fuer Informatik, Dagstuhl, DEU, 2017).

[27] Frank Arute, Kunal Arya, Ryan Babbush, Dave Bacon, Joseph C. Bardin, Rami Barends, Rupak Biswas, Sergio Boixo, Fernando G. S. L. Blandao, David A. Buell, Brian Burkett, Yu Chen, Zijun Chen, Ben Chiaro, Roberto Collins, William Courtney, Andrew Dunsworth, Edward Farhi, Brooks Foxen,

Austin Fowler, Craig Gidney, Marissa Giustina, Rob Graff, Keith Guerin, Steve Habegger, Matthew P. Harrigan, Michael J. Hartmann, Alan Ho, Markus Hoffmann, Trent Huang, Travis S. Humble, Sergei V. Isakov, Evan Jeffrey, Zhang Jiang, Dvir Kafri, Kostyantyn Kechedzhi, Julian Kelly, Paul V. Klimov, Sergey Knysh, Alexander Korotkov, Fedor Kostritsa, David Landhuis, Mike Lindmark, Erik Lucero, Dmitry Lyakh, Salvatore Mandrà, Jarrod R. McClean, Matthew McEwen, Anthony Megrant, Xiao Mi, Kristel Michelsen, Masoud Mohseni, Josh Mutus, Ofer Naaman, Matthew Neeley, Charles Neill, Murphy Yuezhen Niu, Eric Ostby, Andre Petukhov, John C. Platt, Chris Quintana, Eleanor G. Rieffel, Pedram Roushan, Nicholas C. Rubin, Daniel Sank, Kevin J. Satzinger, Vadim Smelyanskiy, Kevin J. Sung, Matthew D. Trevithick, Amit Vainsencher, Benjamin Villalonga, Theodore White, Z. Jamie Yao, Ping Yeh, Adam Zalcman, Hartmut Neven, and John M. Martinis, “Quantum supremacy using a programmable superconducting processor,” *Nature* **574**, 505–510 (2019).

[28] Yulin Wu, Wan-Su Bao, Sirui Cao, Fusheng Chen, Ming-Cheng Chen, Xiawei Chen, Tung-Hsun Chung, Hui Deng, Yajie Du, Daojin Fan, Ming Gong, Cheng Guo, Chu Guo, Shaojun Guo, Lianchen Han, Linyin Hong, He-Liang Huang, Yong-Heng Huo, Liping Li, Na Li, Shaowei Li, Yuan Li, Futian Liang, Chun Lin, Jin Lin, Haoran Qian, Dan Qiao, Hao Rong, Hong Su, Lihua Sun, Liangyuan Wang, Shiyu Wang, Dachao Wu, Yu Xu, Kai Yan, Weifeng Yang, Yang Yang, Yangsen Ye, Jiahui Yin, Chong Ying, Jiale Yu, Chen Zha, Cha Zhang, Haibin Zhang, Kaili Zhang, Yiming Zhang, Han Zhao, Youwei Zhao, Liang Zhou, Qingling Zhu, Chao-Yang Lu, Cheng-Zhi Peng, Xiaobo Zhu, and Jian-Wei Pan, “Strong quantum computational advantage using a superconducting quantum processor,” *Phys. Rev. Lett.* **127**, 180501– (2021).

[29] Han-Sen Zhong, Hui Wang, Yu-Hao Deng, Ming-Cheng Chen, Li-Chao Peng, Yi-Han Luo, Jian Qin, Dian Wu, Xing Ding, Yi Hu, Peng Hu, Xiao-Yan Yang, Wei-Jun Zhang, Hao Li, Yuxuan Li, Xiao Jiang, Lin Gan, Guangwen Yang, Lixing You, Zhen Wang, Li Li, Nai-Le Liu, Chao-Yang Lu, and Jian-Wei Pan, “Quantum computational advantage using photons,” *Science* **370**, 1460–1463 (2020).

[30] Han-Sen Zhong, Yu-Hao Deng, Jian Qin, Hui Wang, Ming-Cheng Chen, Li-Chao Peng, Yi-Han Luo, Dian Wu, Si-Qiu Gong, Hao Su, Yi Hu, Peng Hu, Xiao-Yan Yang, Wei-Jun Zhang, Hao Li, Yuxuan Li, Xiao Jiang, Lin Gan, Guangwen Yang, Lixing You, Zhen Wang, Li Li, Nai-Le Liu, Jelmer J. Renema, Chao-Yang Lu, and Jian-Wei Pan, “Phase-programmable gaussian boson sampling using stimulated squeezed light,” *Phys. Rev. Lett.* **127**, 180502– (2021).

[31] A. Morvan, B. Villalonga, X. Mi, S. Mandrà, A. Bengtsson, P. V. Klimov, Z. Chen, S. Hong, C. Erickson, I. K. Drozdov, J. Chau, G. Laun, R. Movassagh, A. Asfaw, L. T. A. N. Brandão, R. Peralta, D. Abanin, R. Acharya, R. Allen, T. I. Andersen, K. Anderson, M. Ansmann, F. Arute, K. Arya, J. Atalaya, J. C. Bardin, A. Bilmes, G. Bortoli, A. Bourassa, J. Bovaird, L. Brill, M. Broughton, B. B. Buckley, D. A. Buell, T. Burger, B. Burkett, N. Bushnell, J. Campero, H. S. Chang, B. Chiaro, D. Chik, C. Chou, J. Cogan, R. Collins, P. Conner, W. Courtney, A. L. Crook, B. Curtin, D. M. Debroy, A. Del Toro Barba, S. Demura, A. Di Paolo, A. Dunswoth, L. Faoro, E. Farhi, R. Fatemi, V. S. Ferreira, L. Flores Burgos, E. Forati, A. G. Fowler, B. Foxen, G. Garcia, E. Genois, W. Giang, C. Gidney, D. Gilboa, M. Giustina, R. Gosula, A. Grajales Dau, J. A. Gross, S. Habegger, M. C. Hamilton, M. Hansen, M. P. Harrigan, S. D. Harrington, P. Heu, M. R. Hoffmann, T. Huang, A. Huff, W. J. Huggins, L. B. Ioffe, S. V. Isakov, J. Iveland, E. Jeffrey, Z. Jiang, C. Jones, P. Juhas, D. Kafri, T. Khattar, M. Khezri, M. Kieferová, S. Kim, A. Kitaev, A. R. Klots, A. N. Korotkov, F. Kostritsa, J. M. Kreikebaum, D. Landhuis, P. Laptev, K. M. Lau, L. Laws, J. Lee, K. W. Lee, Y. D. Lensky, B. J. Lester, A. T. Lill, W. Liu, A. Locharla, F. D. Malone, O. Martin, S. Martin, J. R. McClean, M. McEwen, K. C. Miao, A. Mieszala, S. Montazeri, W. Mruczkiewicz, O. Naaman, M. Neeley, C. Neill, A. Nersisyan, M. Newman, J. H. Ng, A. Nguyen, M. Nguyen, M. Yuezhen Niu, T. E. O’Brien, S. Omonije, A. Opremcak, A. Petukhov, R. Potter, L. P. Pryadko, C. Quintana, D. M. Rhodes, C. Rocque, P. Roushan, N. C. Rubin, N. Saei, D. Sank, K. Sankaragomathi, K. J. Satzinger, H. F. Schurkus, C. Schuster, M. J. Shearn, A. Shorter, N. Shutty, V. Shvarts, V. Sivak, J. Skrzyni, W. C. Smith, R. D. Somma, G. Sterling, D. Strain, M. Szalay, D. Thor, A. Torres, G. Vidal, C. Vollgraff Heidweiller, T. White, B. W. K. Woo, C. Xing, Z. J. Yao, P. Yeh, J. Yoo, G. Young, A. Zalcman, Y. Zhang, N. Zhu, N. Zobrist, E. G. Rieffel, R. Biswas, R. Babush, D. Bacon, J. Hilton, E. Lucero, H. Neven, A. Megrant, J. Kelly, I. Aleiner, V. Smelyanskiy, K. Kechedzhi, Y. Chen, and S. Boixo, “Phase transition in random circuit sampling,” *arXiv e-prints* (2023), arXiv:2304.11119 [quant-ph].

[32] C. Figgatt, D. Maslov, K. A. Landsman, N. M. Linke, S. Debnath, and C. Monroe, “Complete 3-Qubit Grover search on a programmable quantum computer,” *Nat. Commun.* **8**, 1–9 (2017).

[33] K. Wright, K. M. Beck, S. Debnath, J. M. Amini, Y. Nam, N. Grzesiak, J.-S. Chen, N. C. Pisenti, M. Chmielewski, C. Collins, K. M. Hudek, J. Mizrahi, J. D. Wong-Campos, S. Allen, J. Apisdorf, P. Solomon, M. Williams, A. M. Ducore, A. Blinov, S. M. Kreikemeier, V. Chaplin, M. Keesan, C. Monroe, and J. Kim, “Benchmarking an 11-qubit quantum computer,” *Nat. Commun.* **10**, 5464 (2019).

[34] Tanay Roy, Sumeru Hazra, Suman Kundu, Madhavi Chand, Meghan P. Patankar, and R. Vijay, “Programmable Superconducting Processor with Native Three-Qubit Gates,” *Phys. Rev. Applied* **14**, 014072 (2020).

[35] Elijah Pelofske, Andreas Bartschi, and Stephan Eidenbenz, “Quantum volume in practice: What users can expect from nisq devices,” *IEEE Transactions on Quantum Engineering* **3**, 1–19 (2022).

[36] T. Lubinski, S. Johri, P. Varosy, J. Coleman, L. Zhao, J. Necaise, C. H. Baldwin, K. Mayer, and T. Proctor, “Application-oriented performance benchmarks for quantum computing,” *IEEE Transactions on Quantum Engineering* **4**, 1–32 (2023).

[37] Boaz Barak, Chi-Ning Chou, and Xun Gao, “Spoofing Linear Cross-Entropy Benchmarking in Shallow Quantum Circuits,” in *12th Innovations in Theoretical Computer Science Conference (ITCS 2021)*, Leibniz International Proceedings in Informatics (LIPIcs), Vol. 185, edited by James R. Lee (Schloss Dagstuhl–Leibniz-Zentrum für Informatik, Dagstuhl, Germany, 2021) pp. 30:1–30:20.

[38] Alexander Zlokapa, Benjamin Villalonga, Sergio Boixo, and Daniel A. Lidar, “Boundaries of quantum supremacy via random circuit sampling,” *npj Quantum Information* **9**, 36 (2023).

[39] Dorit Aharonov, Xun Gao, Zeph Landau, Yunchao Liu, and Umesh Vazirani, “A polynomial-time classical algorithm for noisy random circuit sampling,” in *Proceedings of the 55th Annual ACM Symposium on Theory of Computing*, STOC 2023 (Association for Computing Machinery, New York, NY, USA, 2023) pp. 945–957.

[40] Troels F. Ronnow, Zhihui Wang, Joshua Job, Sergio Boixo, Sergei V. Isakov, David Wecker, John M. Martinis, Daniel A. Lidar, and Matthias Troyer, “Defining and detecting quantum

speedup,” *Science* **345**, 420–424 (2014).

[41] Bibek Pokharel and Daniel A. Lidar, “Demonstration of algorithmic quantum speedup,” *Physical Review Letters* **130**, 210602– (2023).

[42] Lorenza Viola and Seth Lloyd, “Dynamical suppression of decoherence in two-state quantum systems,” *Phys. Rev. A* **58**, 2733–2744 (1998).

[43] Lorenza Viola, Emanuel Knill, and Seth Lloyd, “Dynamical decoupling of open quantum systems,” *Physical Review Letters* **82**, 2417–2421 (1999).

[44] Paolo Zanardi, “Symmetrizing evolutions,” *Physics Letters A* **258**, 77–82 (1999).

[45] Bibek Pokharel, Namit Anand, Benjamin Fortman, and Daniel A. Lidar, “Demonstration of fidelity improvement using dynamical decoupling with superconducting qubits,” *Phys. Rev. Lett.* **121**, 220502 (2018).

[46] Alexandre M. Souza, “Process tomography of robust dynamical decoupling with superconducting qubits,” *Quantum Information Processing* **20**, 237 (2021).

[47] Vinay Tripathi, Huo Chen, Mostafa Khezri, Ka-Wa Yip, E. M. Levenson-Falk, and Daniel A. Lidar, “Suppression of crosstalk in superconducting qubits using dynamical decoupling,” *Physical Review Applied* **18**, 024068– (2022).

[48] Petar Jurcevic, Ali Javadi-Abhari, Lev S. Bishop, Isaac Lauer, Daniela F. Bogorin, Markus Brink, Lauren Capelluto, Oktay Günlük, Toshinari Itoko, Naoki Kanazawa, Abhinav Kandala, George A. Keefe, Kevin Krsulich, William Landers, Eric P. Lewandowski, Douglas T. McClure, Giacomo Nannicini, Adinath Narasgond, Hasan M. Nayfeh, Emily Pritchett, Mary Beth Rothwell, Srikanth Srinivasan, Neereja Sundaresan, Cindy Wang, Ken X. Wei, Christopher J. Wood, Jeng-Bang Yau, Eric J. Zhang, Oliver E. Dial, Jerry M. Chow, and Jay M. Gambetta, “Demonstration of quantum volume 64 on a superconducting quantum computing system,” *Quantum Sci. Technol.* **6**, 025020 (2021).

[49] 2022 IEEE International Symposium on High-Performance Computer Architecture (HPCA) (2022).

[50] R. Jozsa, “Quantum factoring, discrete logarithms, and the hidden subgroup problem,” *Computing in Science & Engineering* **3**, 34–43 (2001).

[51] Guangya Cai and Daowen Qiu, “Optimal separation in exact query complexities for simon’s problem,” *Journal of Computer and System Sciences* **97** (2018), 10.1016/j.jcss.2018.05.001.

[52] N. J. A. Sloane, “The On-Line Encyclopedia of Integer Sequences: Erdős-Borwein constant,” (2001).

[53] Nic Ezzell, Bibek Pokharel, Lina Tewala, Gregory Quiroz, and Daniel A. Lidar, “Dynamical decoupling for superconducting qubits: A performance survey,” *Physical Review Applied* **20**, 064027– (2023).

[54] Zeyuan Zhou, Ryan Sitler, Yasuo Oda, Kevin Schultz, and Gregory Quiroz, “Quantum crosstalk robust quantum control,” *Physical Review Letters* **131**, 210802– (2023).

[55] Genko T. Genov, Daniel Schraft, Nikolay V. Vitanov, and Thomas Halfmann, “Arbitrarily accurate pulse sequences for robust dynamical decoupling,” *Physical Review Letters* **118**, 133202– (2017).

[56] Gregory Quiroz and Daniel A. Lidar, “Optimized dynamical decoupling via genetic algorithms,” *Phys. Rev. A* **88**, 052306– (2013).

[57] Hans Zantema, “Complexity of Simon’s problem in classical sense,” *arXiv e-prints* (2022), 2211.01776.

[58] Patricio V Poblete, J Ian Munro, and Thomas Papadakis, “The binomial transform and the analysis of skip lists,” *Theoretical computer science* **352**, 136–158 (2006).

[59] Kristan Temme, Sergey Bravyi, and Jay M. Gambetta, “Error mitigation for short-depth quantum circuits,” *Physical Review Letters* **119**, 180509– (2017).

[60] Siddarth Srinivasan, Bibek Pokharel, Gregory Quiroz, and Byron Boots, “Scalable measurement error mitigation via iterative bayesian unfolding,” *arXiv e-prints* (2022), 2210.12284.